Chapter 12 Results

12.1 Introduction

Results from this study are in four parts:

- the first part deals with the equilibrium solubility trends of AlN in low and high sulphur low carbon Al-killed hot rolled strip steels during reheating;
- the second part deals with the study of the static recrystallisation behaviour after cold work of these steels in the as-quenched form;
- the third part presents the recrystallisation behaviour in laboratory coiled steels; and
- the last part deals with the nucleation of AlN on MnS and its impact on static recrystallisation in these steels.

12.2 Equilibrium solubility trends of AlN in low and high sulphur Al-killed strip steels

The equilibrium solubility trends of AlN in low and high sulphur low carbon Al-killed strip steels were studied in five steels with sulphur content ranging from 2 ppm to 140 ppm using the TEP technique. The steels were LS2-65, LS10-83, LS70-38, HS130-50 and HS140-104 and their compositions are given in table 10.1. The first numeral figure represents the sulphur and the second the nitrogen content, both in ppm.

The aim of this study was to investigate if the sulphur content does have an effect on the equilibrium solubility of the AlN in these steels and to compare the results from the TEP technique with the results from other workers that used other methods, in particular the Beeghly method.

12.2.1 Effect of soaking time on the dissolution of the AlN

Figure 12.1 shows the evolution of the relative TEP values after isothermally soaking two steels with high and low sulphur content, steels HS140-104 and LS2-65 respectively, at 1150 °C for various times and then quenching them into water. The relative TEP values were taken with reference to the "no dissolution" TEP values at 800 °C as these specimens were given a prior isothermal annealing at 800 °C for 2 hours to precipitate the AlN.

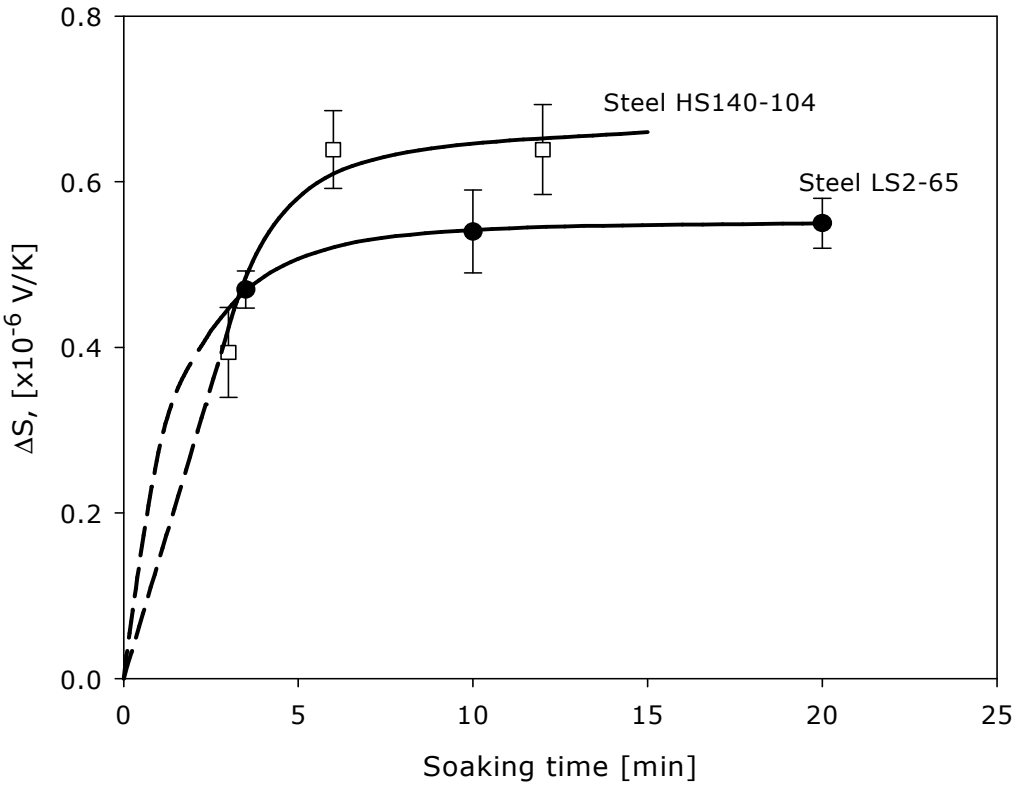

Figure 12.1: Relative TEP measurements ΔS for steels HS140-104 and LS2-65 after soaking for various times at 1150 °C and quenching into water.

The TEP values leveled off after soaking for more than 5 minutes and this was an indication of equilibrium condition in the solubility of the dissolving AlN. An important observation from this study was that equilibrium dissolution of AlN is not affected by the sulphur content in these steels.

12.2.2 Equilibrium solubility trends of AlN in low and high sulphur low carbon Al-killed hot strips during reheating

The TEP results for the equilibrium solubility trend of AlN in austenite are given in table 12.1 and the corresponding curves of relative TEP values versus the soaking temperature are given in figure 12.2 below. The leveling off of the TEP values at higher soaking temperature may indicate the solubility limit of the dissolving AlN and the final relative TEP values are, therefore, dependent on the nitrogen content.

Instead of plotting the relative TEP value ΔS versus the solution temperature as in figure 12.2, the logarithm of the solubility product log[%Al][%N] derived from ΔS through equation 8.7, is plotted against the inverse of the absolute solution temperature in figure 12.3. This data is for 5 to 95 percent AlN dissolution and this was approximated from the sigmoidal curves in figure 12.2. Despite some scatter in the results, an important observation was that the sulphur content did not have a significant effect on the equilibrium solubility trend of AlN as the data points for all the five steels were within the reasonable scatter. It is to be noted that it

was the solubility product of the stoichiometric composition of the AlN that was plotted against the inverse of the absolute temperature in figure 12.3.

The equation from the regression analysis of the plot of the logarithm of the solubility product of the AlN, i.e. Log[%Al][%N], versus the inverse of the absolute solution treatment temperature in figure 12.3, was found to be:

$$\mathrm{Log[\%Al][\%N]} = 2.6 - \frac{9710}{T} \qquad (12.1)$$

where the aluminium and the nitrogen contents are in weight percentage and T is the absolute solution temperature in Kelvin.

In addition, the equilibrium solubility of AlN in steel HS140-104 was modelled by Thermo-Calc and the results are shown in figure 12.4. Curve number 5 in figure 12.4 shows the modelled precipitation behaviour of AlN as the sulphur content is varied with no predicted effect of the sulphur content.

Chapter 12 Results

Table 12.1: TEP measurements for the various steels that were solution treated at different temperatures for 12 minutes and quenched into water. The TEP values were within an error of ± 0.033 μV K^{-1} while the ΔS values were taken relative to the "no dissolution" TEP values at 800°C.

Steel	Solution Temperature [°C] and TEP [μV/K]									
	800	**925**	**1000**	**1050**	**1100**	**1150**	**1200**	**1225**	**1250**	**1290**
HS130-50	9.01		8.734	8.741	8.668	8.61	8.5	8.511	8.68	
$\Delta S = S_{800} - S_i$	0		0.28	0.27	0.35	0.41	0.46	0.45	0.39	
LS10-83	9.15		9.00	8.96	8.80	8.55	8.52	8.50		
$\Delta S = S_{800} - S_i$			0.15	0.19	0.35	0.60	0.63	0.65		
HS140-104	8.63			8.48	8.25	8.28	7.91			7.84
$\Delta S = S_{800} - S_i$				0.15	0.38	0.35	0.72			0.79
LS2-65	8.12	8.10	7.86		7.74	7.65	7.82		7.89	
$\Delta S = S_{800} - S_i$	0.00	0.02	0.25		0.38	0.47	0.30		0.23	
HS90-34	8.99	8.93	8.76		8.78					
$\Delta S = S_{800} - S_i$	0.00	0.06	0.23		0.21					

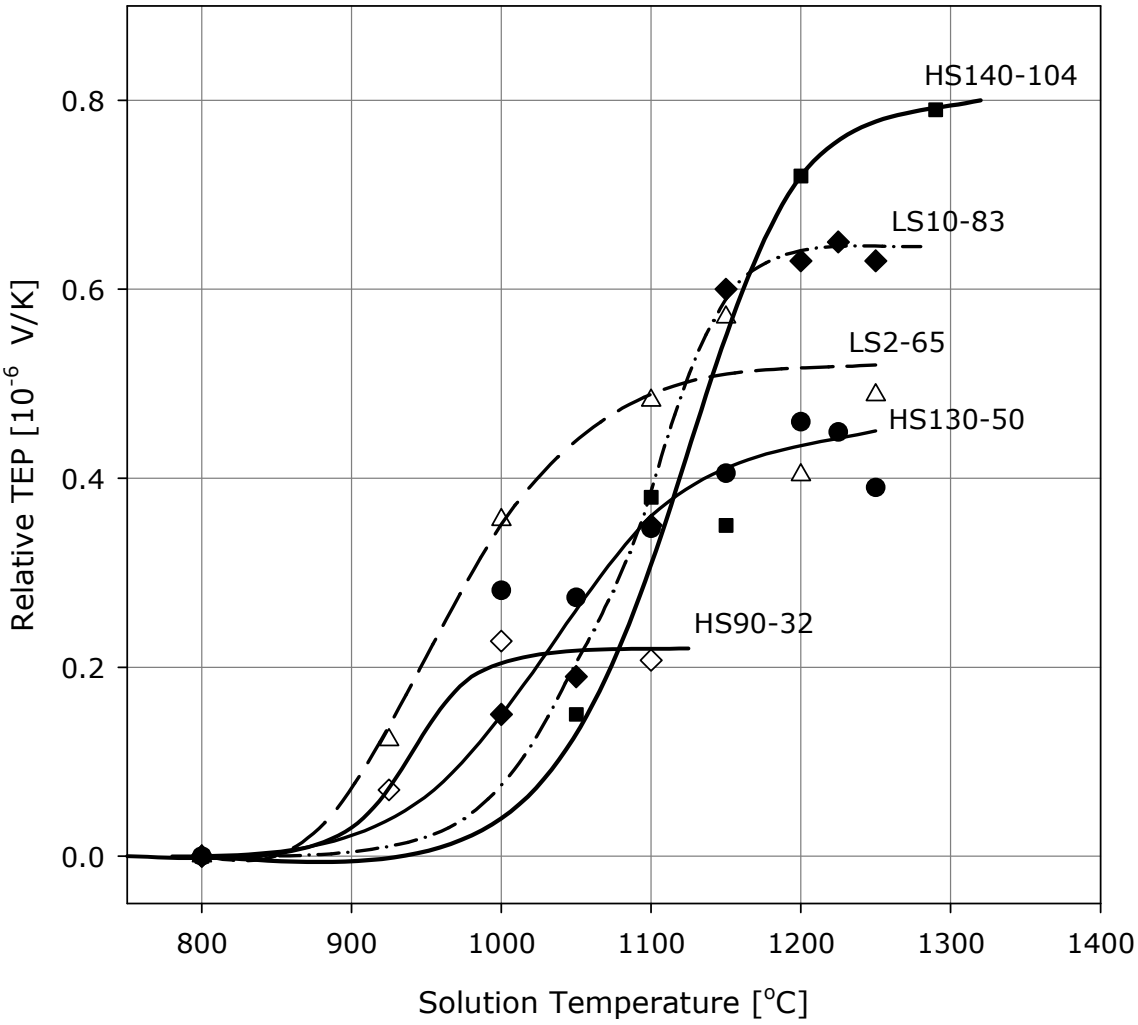

Figure 12.2: Equilibrium solubility trends for AlN in low carbon Al-killed hot rolled strip steels during reheating for the steels which are labeled on corresponding solubility curve.

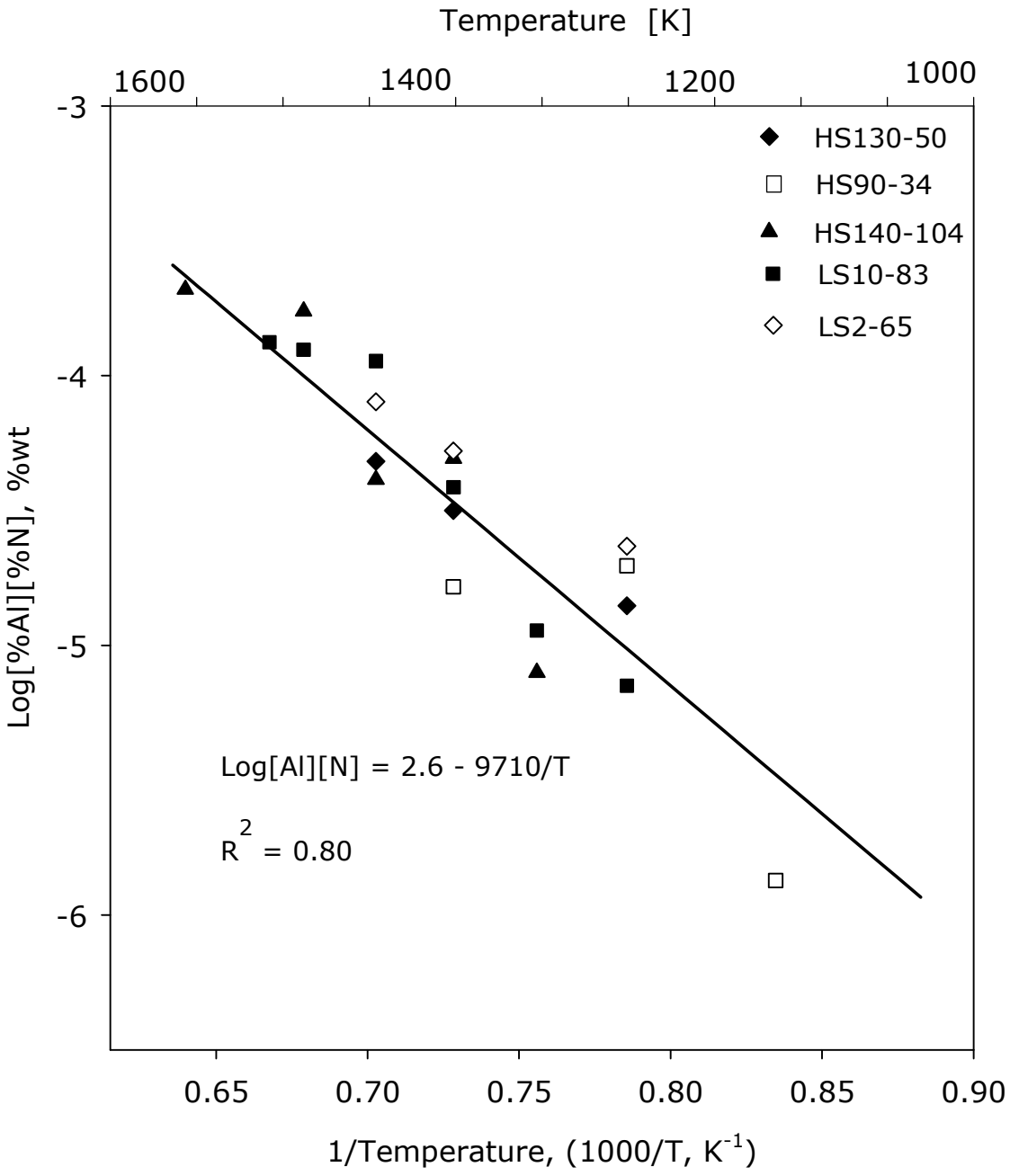

Figure 12.3: The logarithm of the AlN solubility product log[%Al][%N] as a function of the inverse of the absolute solution treatment temperature.

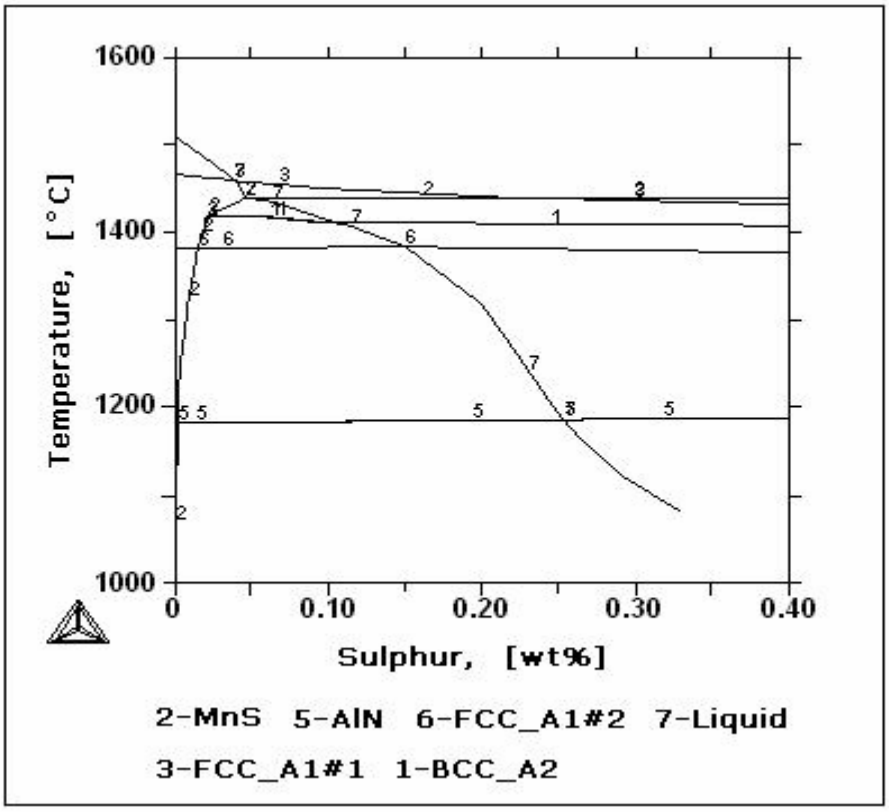

Figure 12.4: Thermo-Calc results for steel HS140-104: note curve number 5 that represents the precipitation of AlN.

12.2.3 Metallographic analysis

The results from the TEP measurements were checked metallographically in order to confirm that the AlN had been fully dissolved. Both extraction carbon replicas and thin foil techniques were used for this. Out of the five steels that were studied by TEP, two steels, one with the highest and the other with the lowest sulphur contents were chosen for metallographic analysis i.e. steels HS140-104 and LS2-65. Figure 12.5 shows micrographs and corresponding EDS spectra for the particles in steels HS140-104 and LS2-65 after solution treatment at 1150 °C, hot rolling

and annealing at 800 °C for 6 hours as shown in the schematic diagram in figure 10.1. After isothermal annealing at 800 °C for 6 hours, the AlN precipitated into coarse cuboids and fine round particles.

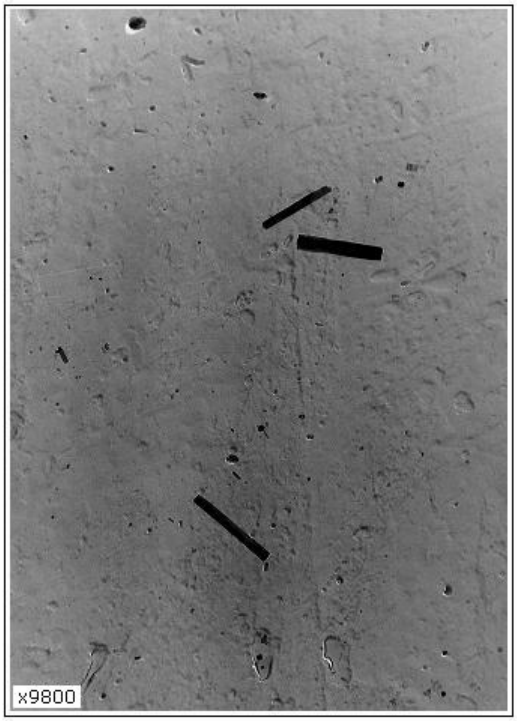

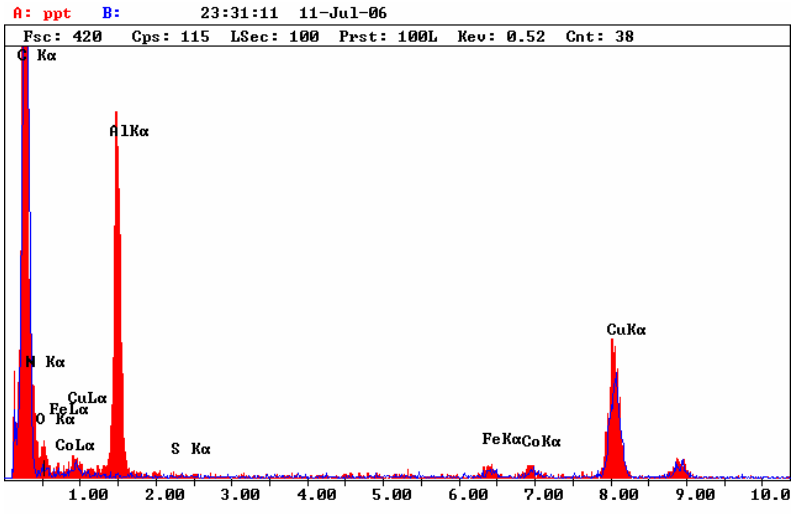

(a)

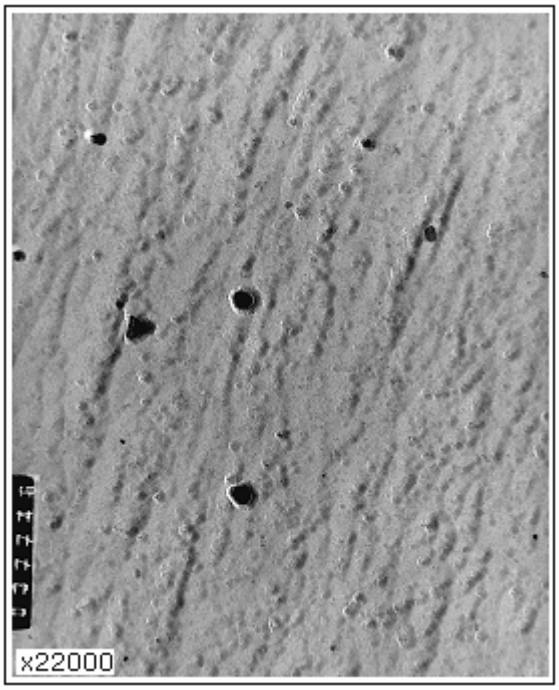

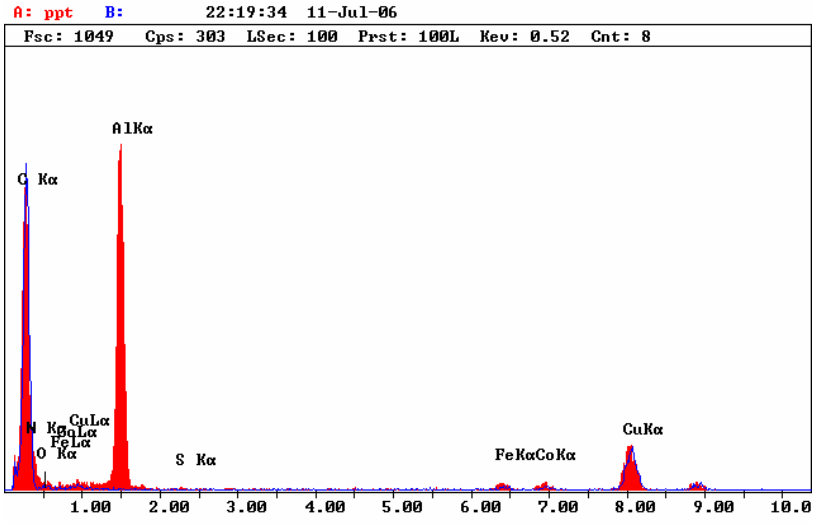

(b)

Figure 12.5: Micrographs and the corresponding EDS spectra for the steels (a) HS140-104 and (b) LS2-65 which were hot rolled, cooled to room temperature and then isothermally annealed at 800 °C for 6 hours and then quenched into water.

Extraction carbon replicas were also prepared for specimens that were only solution treated at 1150 °C for 12 minutes and water

quenched and their micrographs are shown in figure 12.6. As may be seen in the carbon extraction replicas below, there was partial dissolution of AlN in the higher nitrogen steel HS140-104 (micrograph (a)) while almost complete dissolution in the medium nitrogen steel LS2-65 (micrograph (b)). The particles in micrograph 12.6 (a) were also analysed by the x-ray EDS and were found to be AlN as in figure 12.5 above.

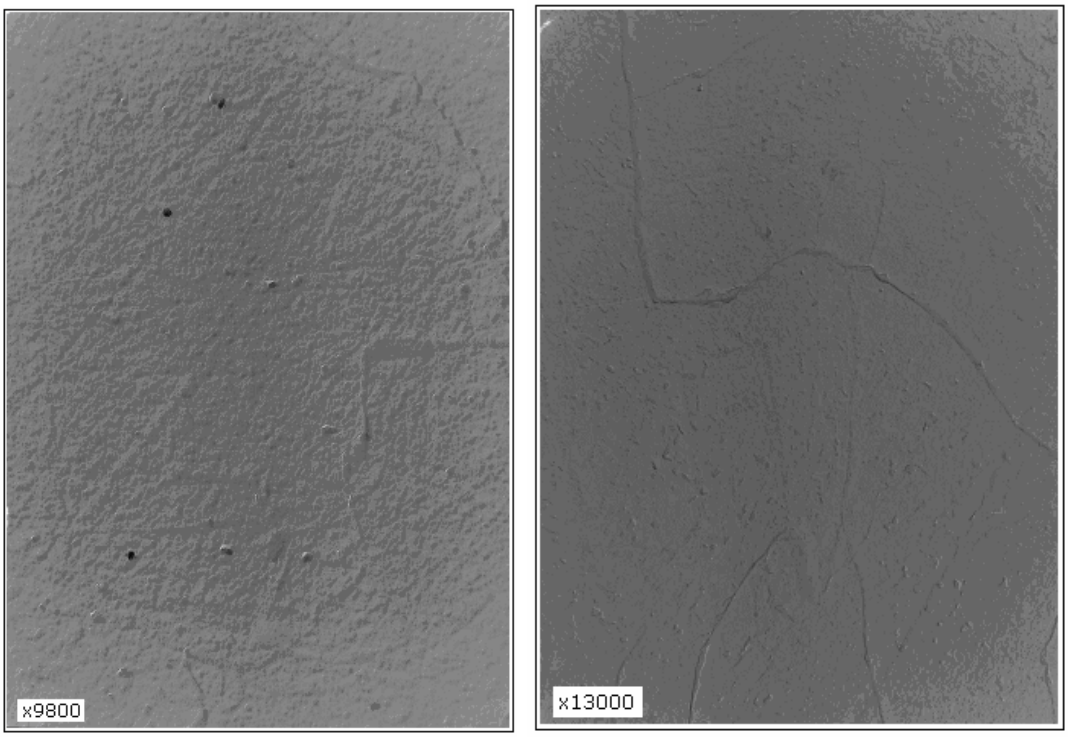

(a) (b)

Figure 12.6: Micrographs for the two steels (a) HS140-104 and (b) LS2-65 after solution treatment at 1150 °C for 12 minutes and quenched into water.

The fact that AlN particles could not be seen in steel LS2-65 did not necessarily mean that there were not any as the extraction carbon replica technique is known to be insensitive to very small

particles and, therefore, TEM thin foils were prepared. Figure 12.7 shows the TEM thin foil results for steel LS2-65 after solution treatment at 1150 °C for 12 minutes and then quenched into water. Some AlN particles (< 30 nm) were observed but they were sporadic. No AlN particles could be observed when the solution treatment temperature was raised to 1200 °C. This meant that the dissolution of AlN in this steel was some where between 1150° and 1200 °C, which was about 50 °C above the temperature determined by the TEP technique.

Similarly, steel HS140-104 was solution treated further at 1250 °C for 12 minutes to dissolve the still remaining AlN at 1150 °C and the results are shown in figure 12.8 i.e. no more AlN was observed after quenching from 1250 °C, instead only Al_2O_3 particles were observed. This observation agreed with the TEP equilibrium solubility results.

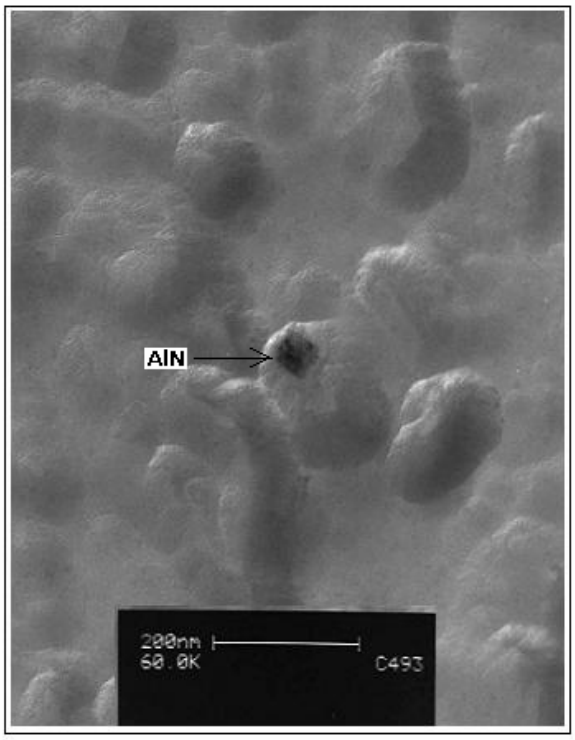

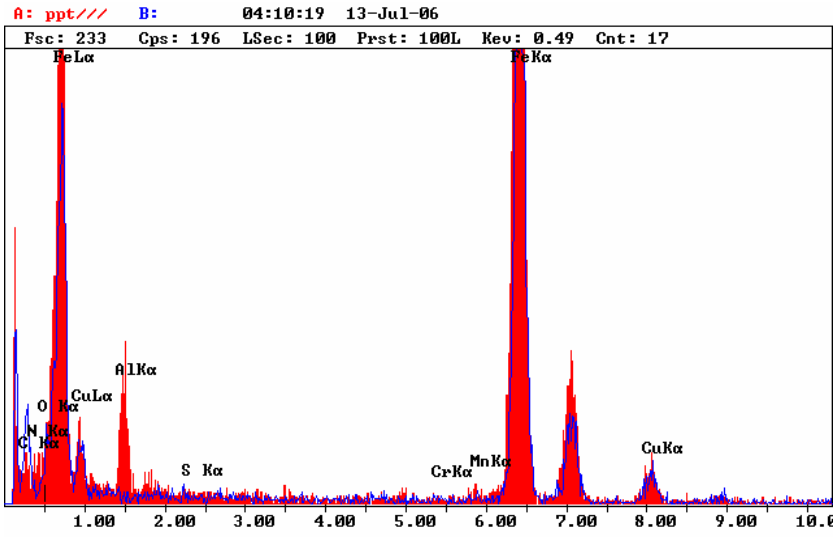

(b)

Figure 12.7: (a) Thin foil micrograph for steel LS2-65 after solution treatment at 1150 °C for 12 minutes and quenching into water and (b) the corresponding EDS spectrum of the single particle in the micrograph.

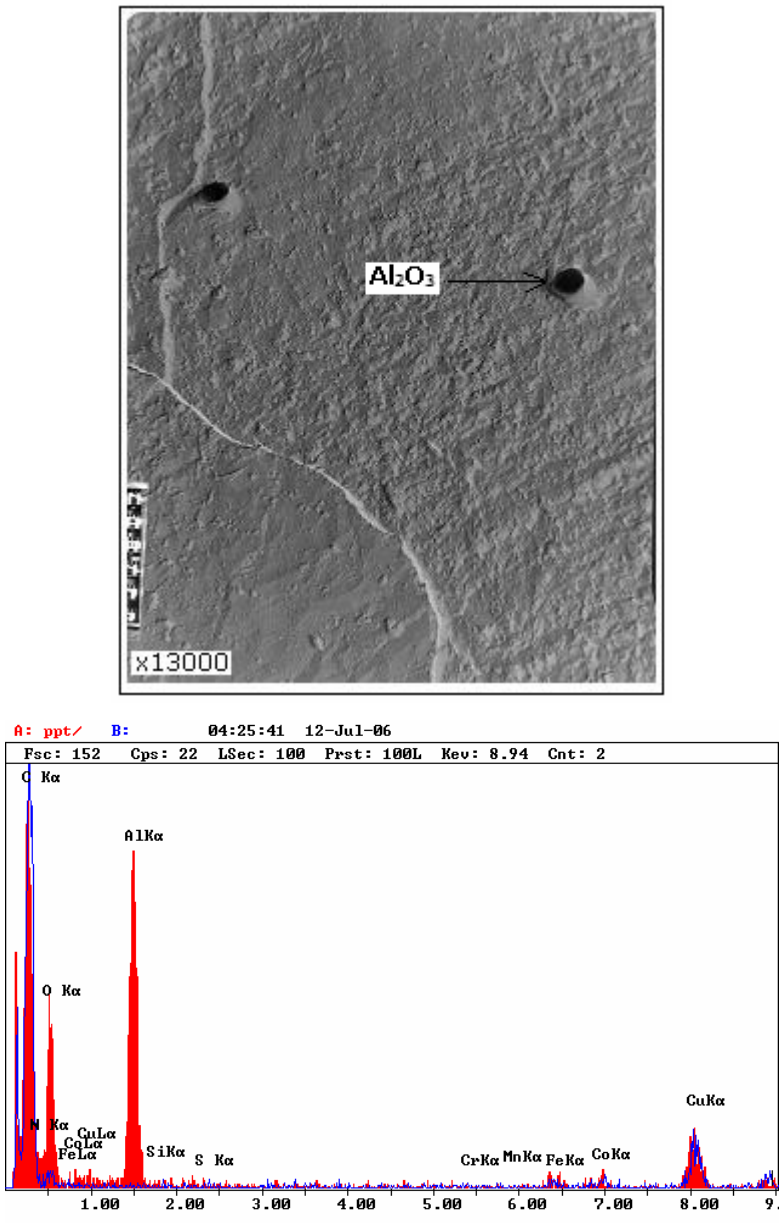

Figure 12.8: Micrograph and corresponding EDS spectrum for the particles which were observed in steel HS140-104 after solution treatment at 1250 °C for 12 minutes and quenching into water.

12.3 Recrystallisation behaviour in the as-quenched condition

The recrystallisation behaviour of low and high sulphur low carbon Al-killed strip steels was studied in steels HS140-104, HS90-12, LS70-38 and LS2-65 with the first digit representing the sulphur content and the second digit the nitrogen content respectively, both in ppm. As mentioned earlier in the experimental procedures, the study was done in two stages. Firstly, the recrystallisation behaviour was investigated in the as-quenched condition in order to observe the effects of both sulphur and nitrogen when they are in solid solution at the start of recrystallisation. Secondly, the study was extended to as-hot rolled and coiled specimens in order to investigate the effect of coiling and the interaction of AlN with the sulphides vis-à-vis the recrystallisation process in the two groups of steels; one with low sulphur content and the other with medium to high sulphur content. The latter set of results will be presented in section 12.4 below.

12.3.1 Progression of the recrystallisation as investigated by metallography

Steels HS140-104, HS90-12, LS70-38 and LS2-65 were solution treated at 1300 °C for 10 minutes and quenched into water and the resulting microstructure was massive ferrite. The as-quenched steels were immediately given a 70 percent cold deformation and, thereafter, isothermally annealed at different temperatures for various times to induce the static recrystallisation.

Chapter 12 Results

The micrographs in figure 12.9 show the progression of the recrystallisation process during isothermal annealing at 610 °C in steel HS140-104 with the light coloured areas the recrystallised regions and the dark ones the non-recrystallised ones. The micrographs in figure 12.9 show that there was no significant change in the recrystallised volume fraction as the isothermal annealing time was extended from 5 to 18 minutes i.e. there was a recrystallisation arrest. The recrystallisation process resumed again after 18 minutes.

Figure 12.10 shows the progression of the recrystallisation process in the same steel HS140-104 but now annealed at 550 °C. No recrystallisation arrest was observed at this annealing temperature.

Figure 12.11 shows the micrographs of the progression of the recrystallisation process in steel HS90-12 with the lowest nitrogen content of 12 ppm. This steel was also solution treated at 1300 °C for 10 minutes, quenched into water, given a 70 percent cold deformation and isothermally annealed at 610 °C for various times. No recrystallisation arrest was observed in this steel.

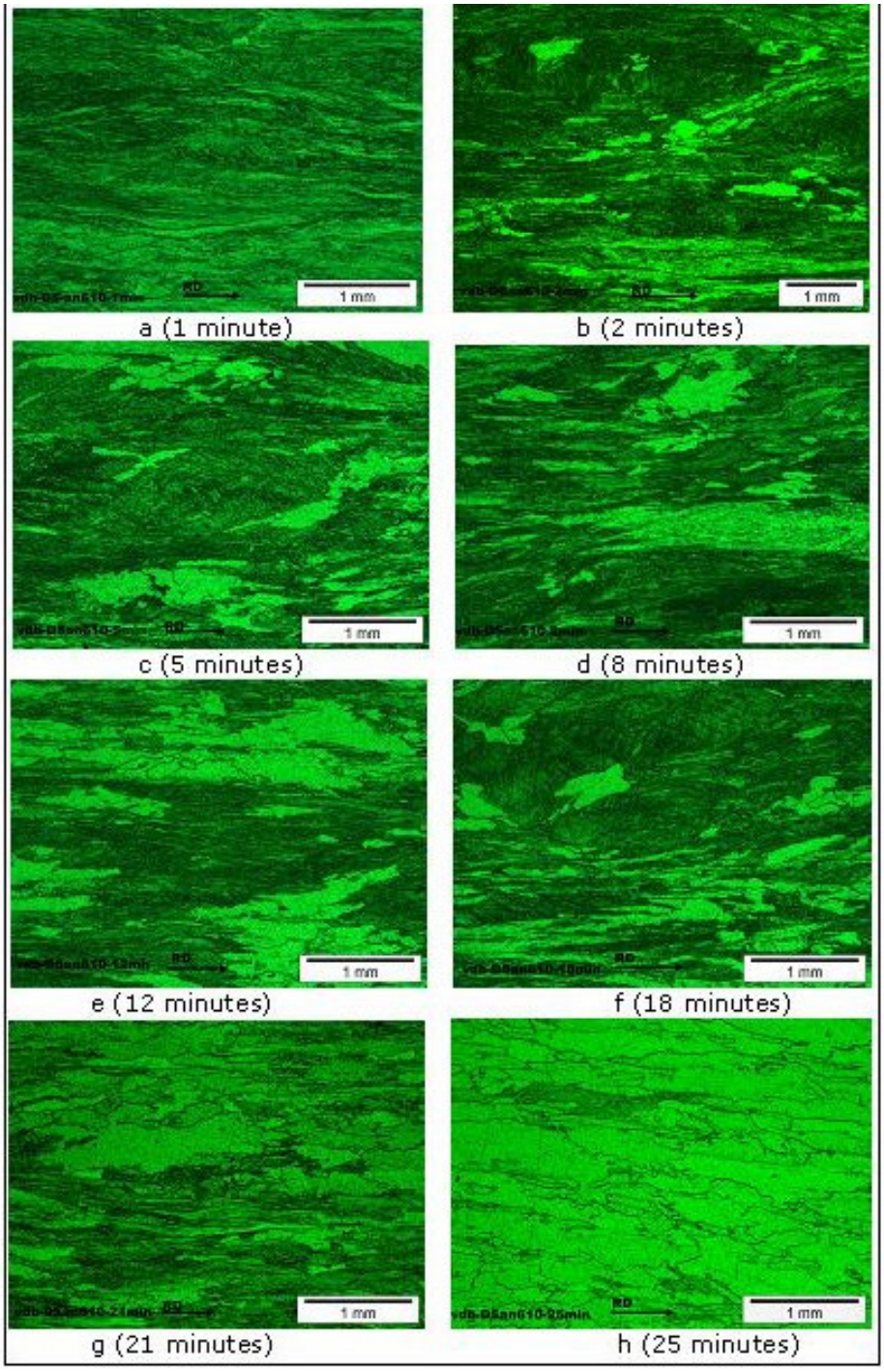

Figure 12.9: Progression of the static recrystallisation in steel HS140-104 after solution treatment at 1300 °C, quenching into water, cold working 70 percent and annealing at 610 °C for various times.

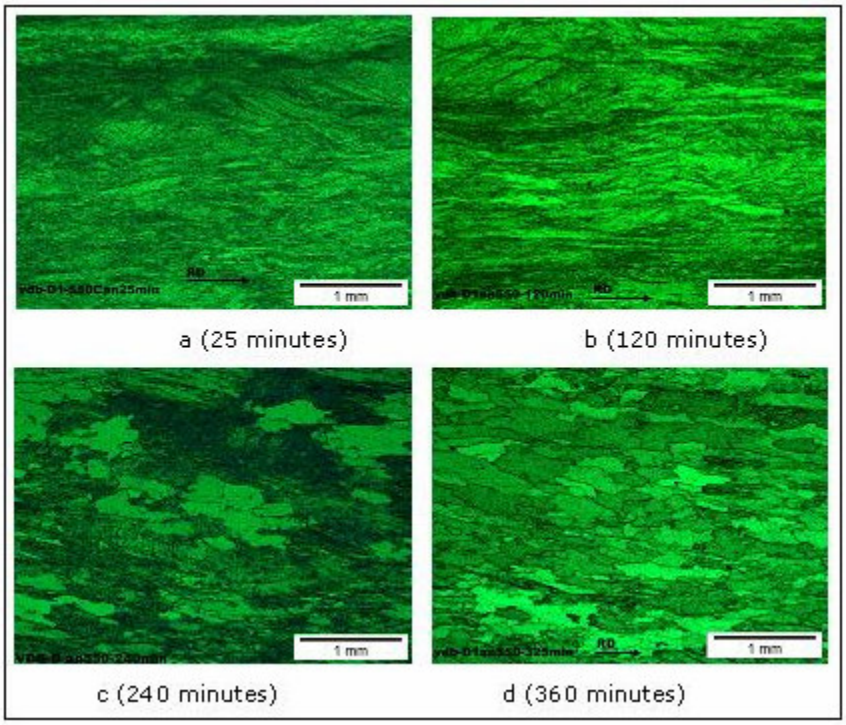

Figure 12.10: Progression of the static recrystallisation in steel HS140-104 after solution treatment at 1300 °C, quenching into water, cold working 70 percent and annealing at 550 °C for various times

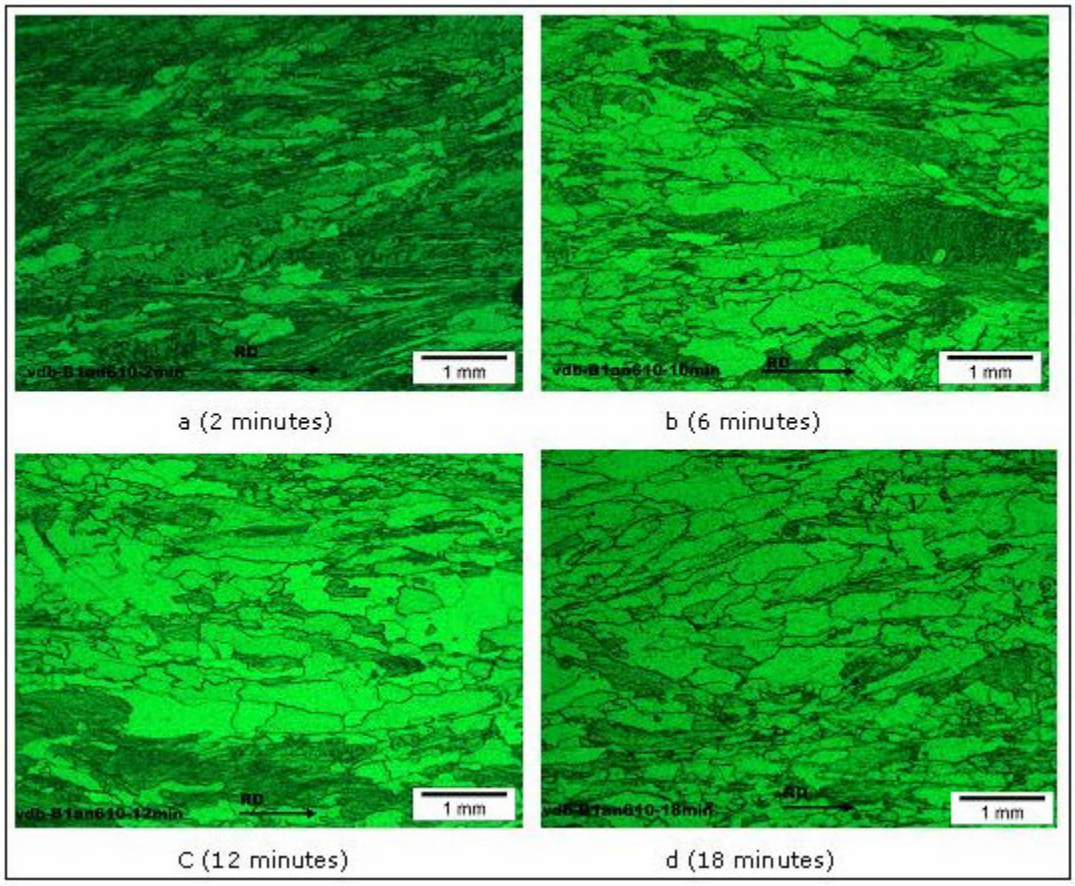

Figure 12.11: Progression of static recrystallisation in steel HS90-12 after solution treatment at 1300 °C, quenching into water, cold working 70 percent and annealing at 610 °C for various times

12.3.2 Quantitative results of the static recrystallisation kinetics in steel HS140-104 in as-quenched condition

In figure 12.12, the recrystallised volume fraction as determined through area analysis micrographic software, is plotted against the isothermal annealing time for various recrystallisation temperatures for steel HS140-104 that was given the treatment as mentioned in section 12.3.1 above. In some cases a clear

region of "recrystallisation arrest" was found as shown collectively by the cross hatched area in figure 12.12.

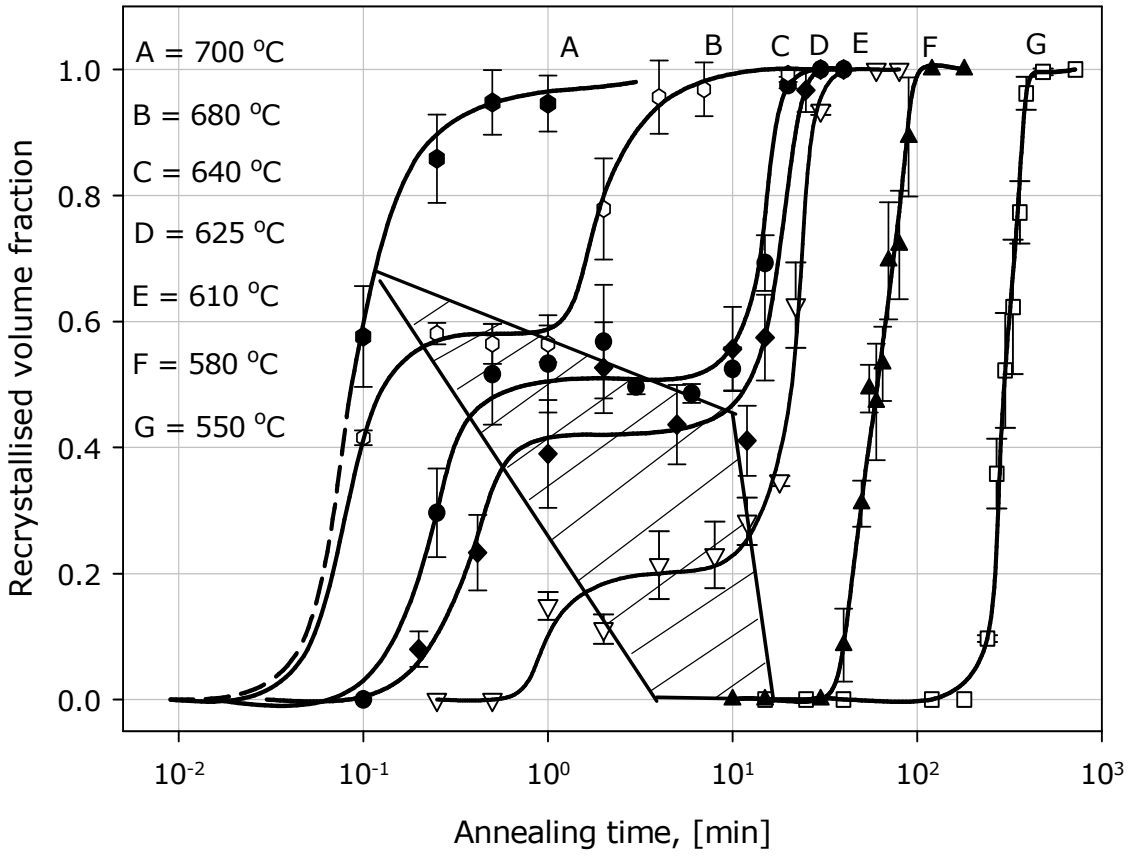

Figure 12.12: Recrystallised volume fraction versus isothermal annealing time for steel HS140-104 after solution treatment at 1300 °C, quenching into water, cold working 70 percent and annealing at various temperatures for various times. The cross hatched area is the recrystallisation arrest region.

Some specimens of steel HS140-104 were also annealed at 450 °C for 30 minutes in order to precipitate the Fe_3C prior to the 70 percent deformation and the recrystallisation annealing. According to Konig et al[44] and Leslie et al[66], see figure 4.2, no AlN is

expected to precipitate at this temperature at shorter annealing times and, therefore, only the cementite would be precipitated. This was done to investigate the possible effects of the carbon (in or out of solid solution) in the as-quenched specimens on the recrystallisation process after cold work. The results are given in figure 12.13 which confirmed that the movement of carbon does not appear to play any role in the kinetics of the recrystallisation process in these steels.

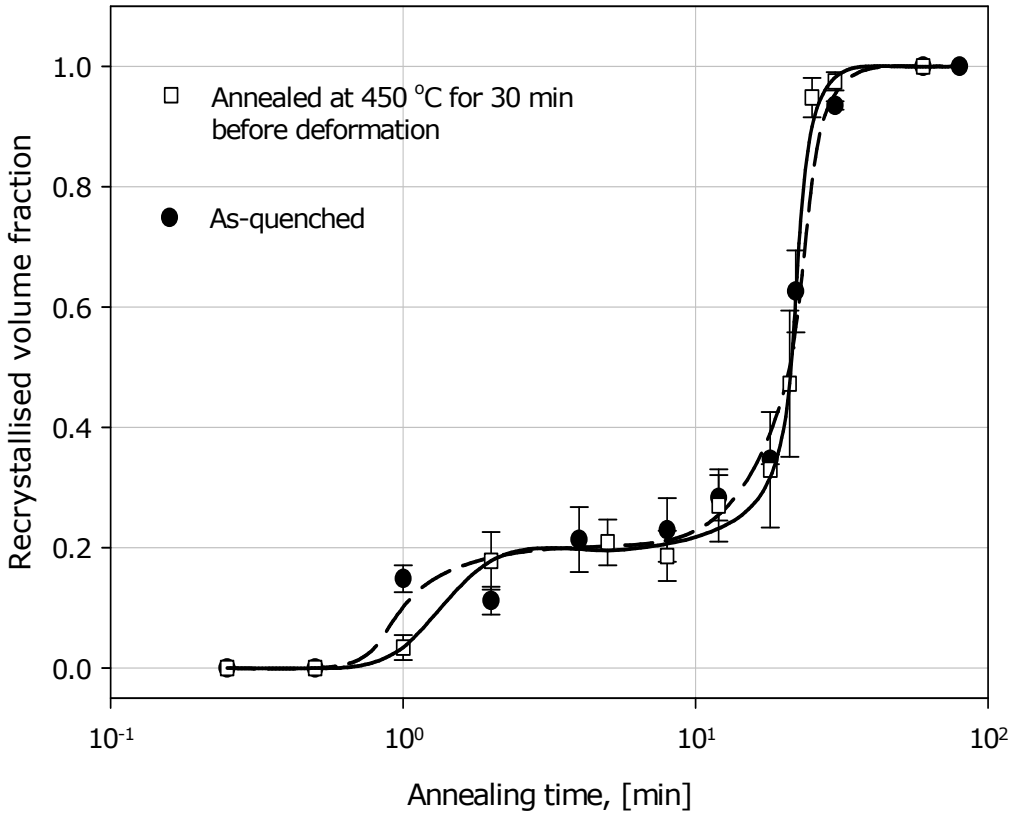

Figure 12.13: Recrystallised volume fraction versus isothermal annealing time for steel HS140-104 that was solution treated at 1300 °C, quenched in water; one annealed at 450 °C for 30 minutes and the other as-quenched, then both cold worked 70 percent and isothermally annealed at 610 °C for various times.

Chapter 12 Results

The log of the inverse of the recrystallisation arrest start time t_{RA} is, therefore, plotted against the inverse of the absolute isothermal annealing temperature in figure 12.14. The apparent activation energy of the process that led to the recrystallisation arrest was derived from the slope of this graph and its value was 230 kJ mol^{-1}. This activation energy is reasonably close to that for the diffusion of aluminium in ferrite which Germaz et al[149] found to be 196.5 kJ mol^{-1}.

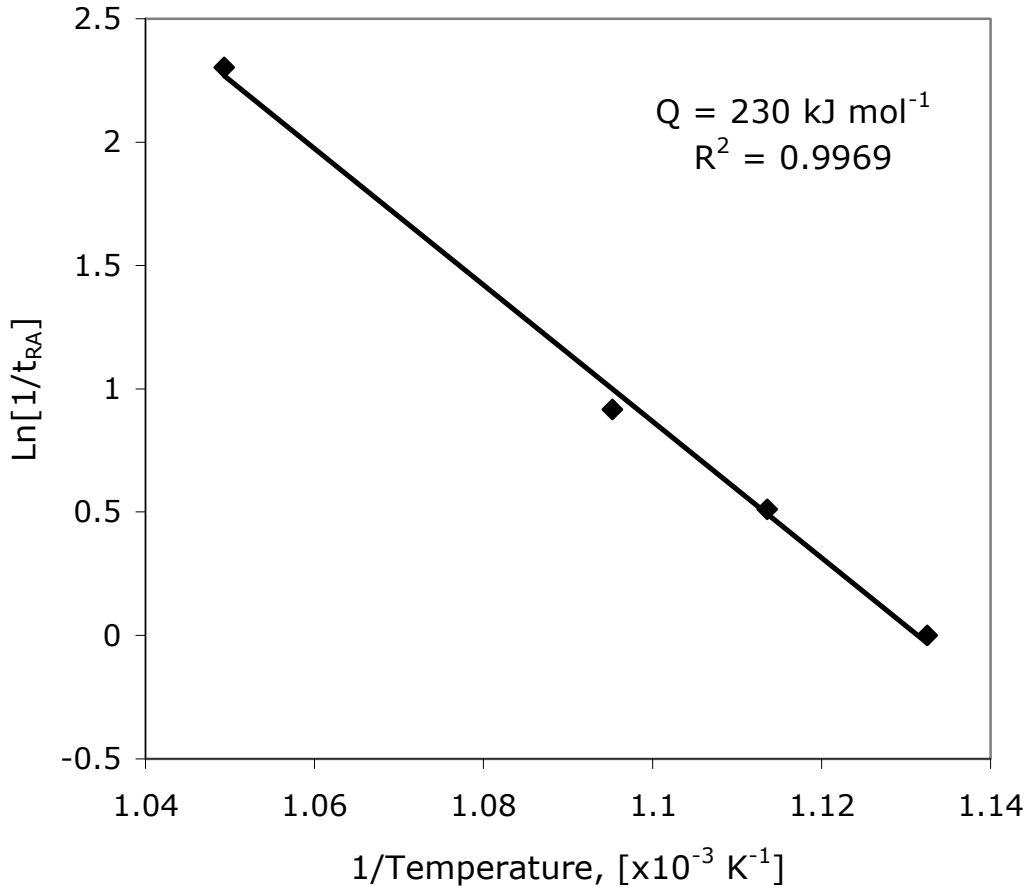

Figure 12.14: The inverse of the recrystallisation arrest start time t_{RA} versus the inverse of the isothermal annealing temperature.

Chapter 12 Results

The Zener-pinning effect start Z_{start} and finish Z_{finish} times observed in figure 12.12 above and plotted separately in figure 12.15 can indirectly be used to measure an estimated AlN precipitation start P_{start} and finish P_{finish} times in these steels. This is, of course, only an approximation measured indirectly by a Zener-like recrystallisation pinning effect which is dictated by the ratio (V_v/r) of AlN particles. For instance, some AlN precipitation may, therefore, already be present before the estimated P_{start} but is merely ineffective due to a very low volume fraction.

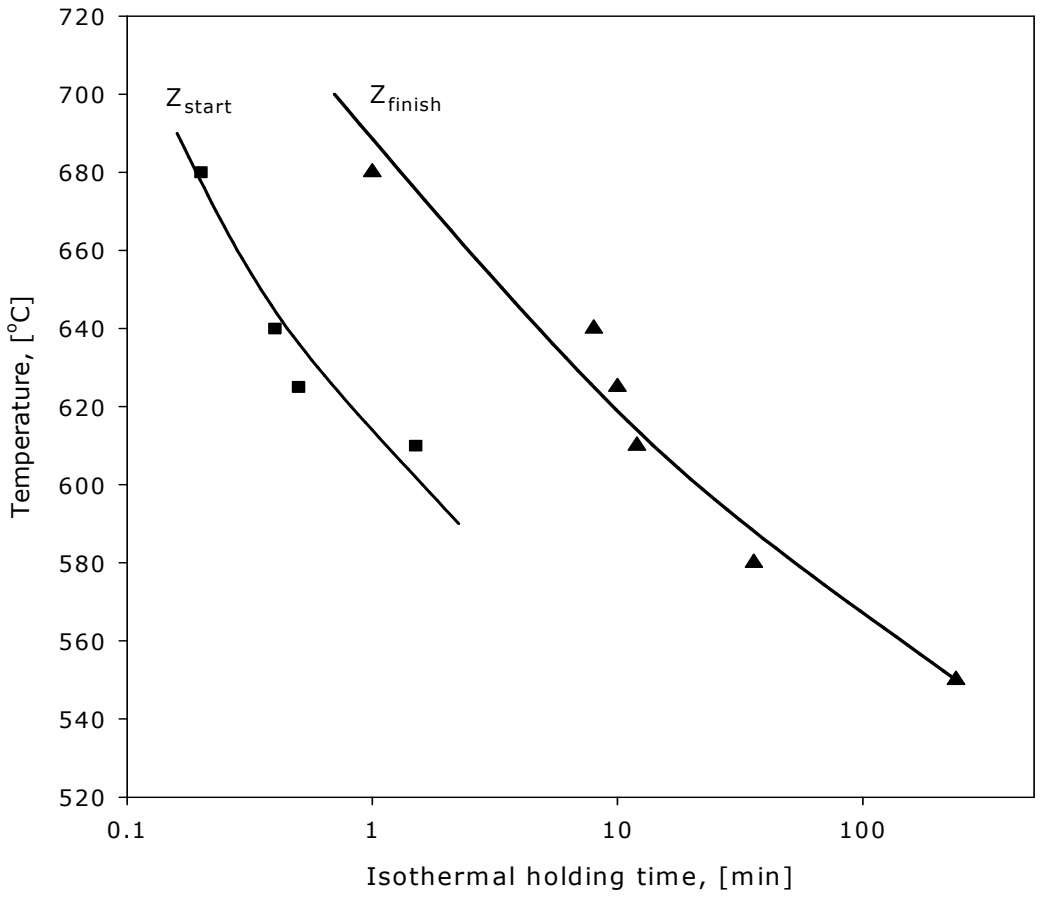

Figure 12.15: The Zener-pinning effect start Z_{start} and finish Z_{finish} times in minutes which were derived from the recrystallisation arrest times in figure 12.12.

12.3.3 Comparison of the recrystallisation kinetics in low and high sulphur content steels in as-quenched condition

The recrystallisation behaviour of four steels, two with low to medium sulphur content (LS2-65 and LS70-38) and the other with medium to high sulphur content (HS90-12 and HS140-104) is compared in figure 12.16. All four steels were solution treated at 1300 °C, quenched into water, cold worked 70 percent and annealed at 610 °C for various times. It is worthwhile observing that, regardless of the nitrogen content, the steels with lower sulphur content in solid solution recrystallised at earlier times compared with the ones with the higher sulphur content.

The Avrami plots for steels LS70-38 and HS90-12 are given in figure 12.17 and it is evident that the sulphur content does not affect the recrystallisation kinetics but rather the incubation period as there was significant no difference in the values of the MAJK exponent n.

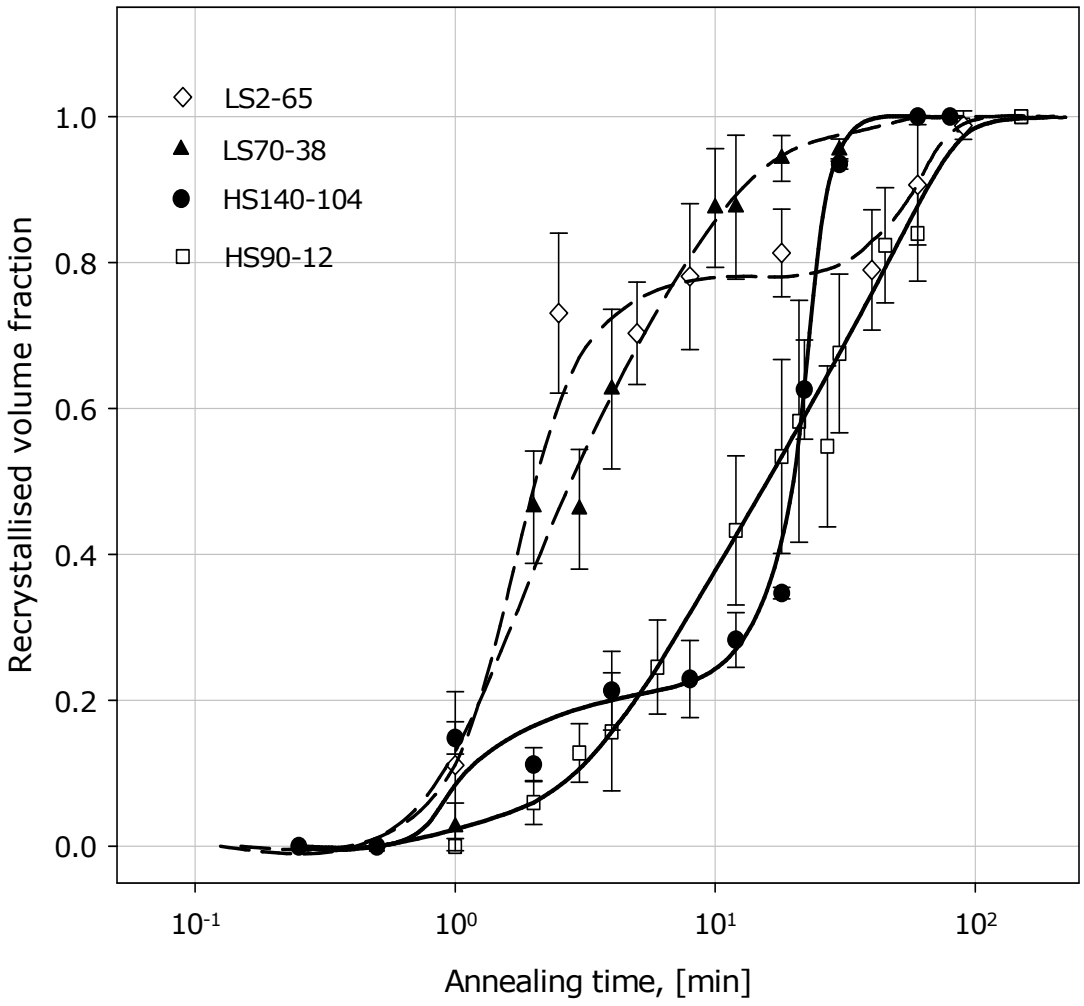

Figure 12.16: The recrystallised volume fraction versus isothermal annealing time for steels LS2-65, LS70-38, HS140-104 and HS90-12 after solution treatment at 1300 °C, water quenching, cold working 70 percent and isothermally annealing at 610 °C for various times.

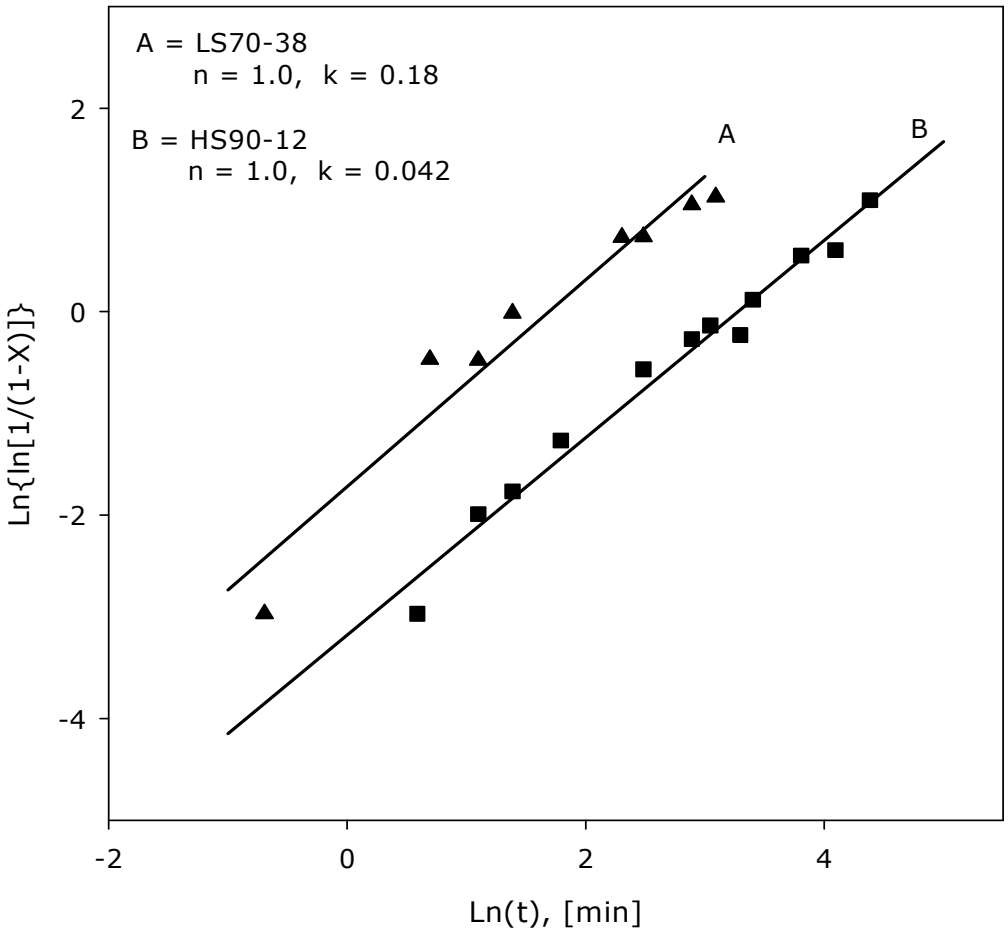

Figure 12.17: Avrami plots for steels LS70-38 and HS90-12 from the data in figure 11.16.

12.4 Recrystallisation behaviour in as-coiled condition

The recrystallisation behaviour of steels HS140-104, LS70-38 and LS2-65 with sulphur contents of 140, 70 and 2 ppm respectively was studied in this series. These three steels were hot rolled and coiled through simulation on the Gleeble 1500^{TM} and details of the process were given in table 11.1 and figure 11.1. The main

variables in these experiments were the coiling temperature (600° and 650 °C) and the sulphur content of the steel.

12.4.1 Quantitative results of the recrystallisation behaviour of the as-coiled hot strips

Figure 12.18 shows the plots of the recrystallised volume fraction versus isothermal annealing time for steels HS140-104, LS70-38 and LS2-65. These steels were coiled in the Gleeble 1500^{TM} at 600 °C and 650 °C, given a cold deformation of 70 percent and isothermally annealed respectively at 600 °C and 650 °C in the lead bath for various times.

The Avrami plots derived from the sigmoidal curves in figure 12.18 are given in figure 12.19. The main observation from these two figures was that, unlike in the as-quenched condition with all the sulphur in solid solution, steels with lower sulphur content recrystallised at later times and this effect was more prominent at the lower coiling temperature of 600 °C.

In figure 12.20, the static recrystallisation time i.e., 5 percent recrystallisation $t_{5\%}$, has been plotted against the corresponding sulphur content of the three steels that were studied in this series. A very pronounced effect of "sluggish" recrystallisation at low sulphur contents and low coiling temperature is apparent, which confirms the differences in recrystallisation behaviour reported within industry from nominally the same product but from different process plants that originally led to this study.

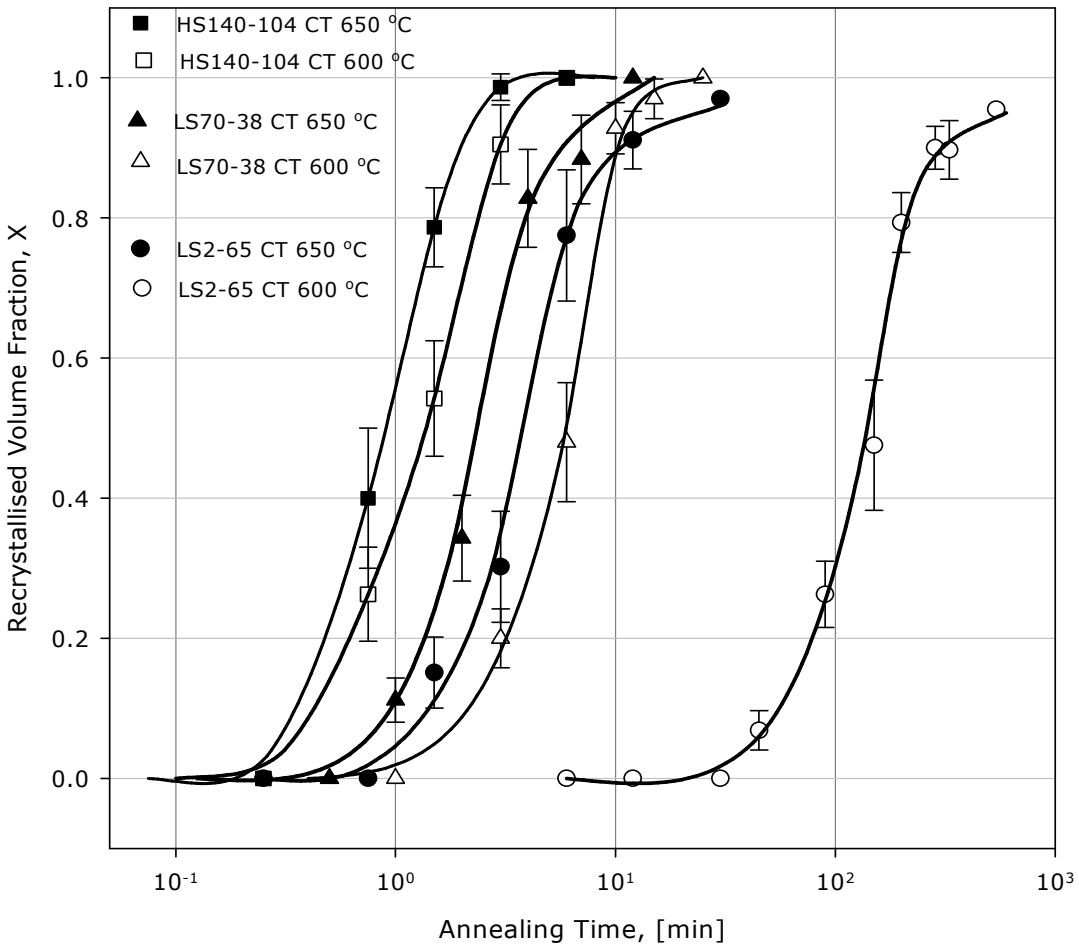

Figure 12.18: Recrystallised volume fraction for steels HS140-104, LS70-38 and LS2-65 which were coiled at 600 °C and 650 °C, cold worked 70 percent and isothermally annealed at 600 °C and 650 °C in a lead bath for various times. CT stands for coiling temperature.

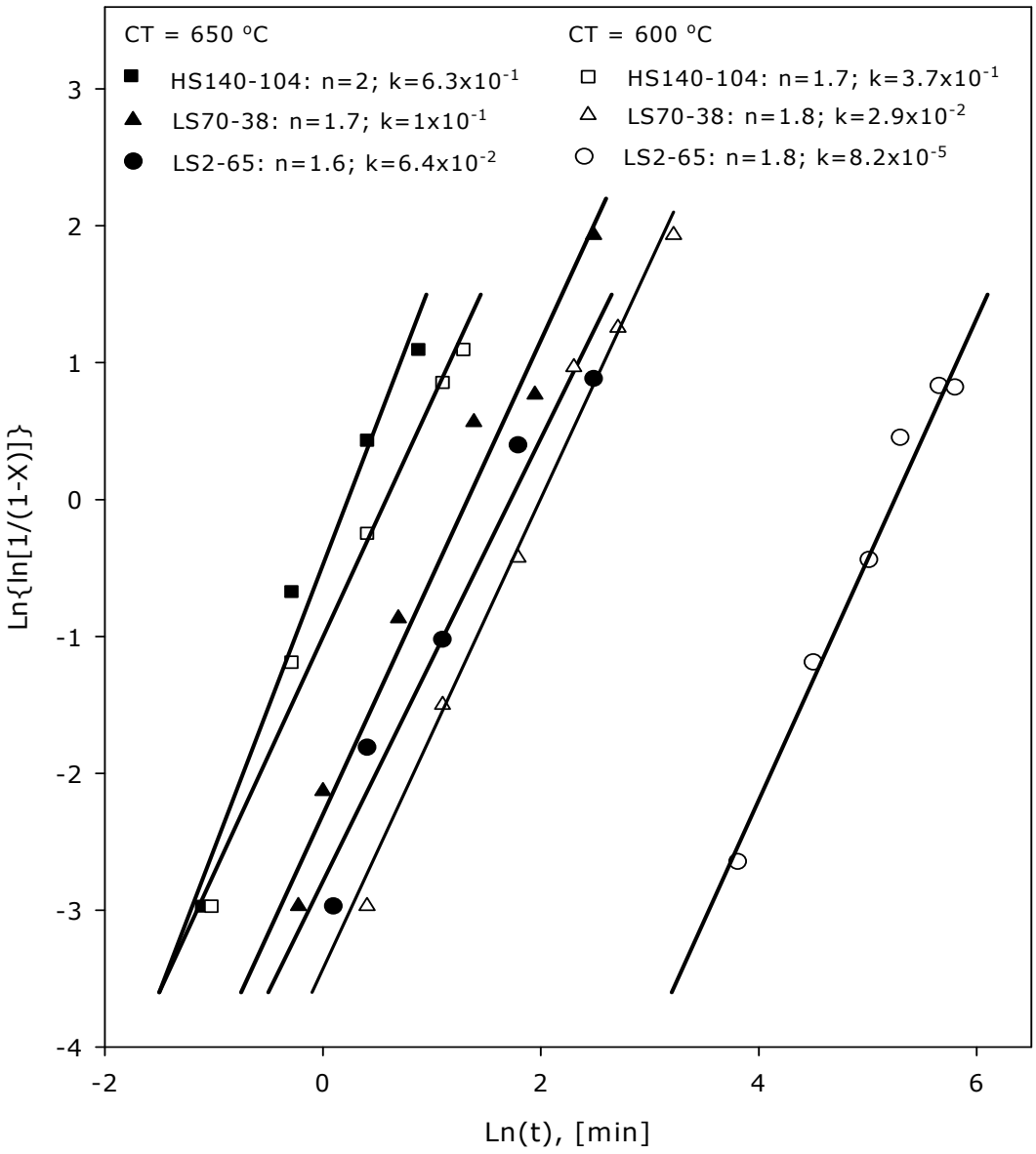

Figure 12.19: Avrami plots from the sigmoidal curves of recrystallised volume fraction versus isothermal annealing time for the steels and treatment given in figure 12.18.

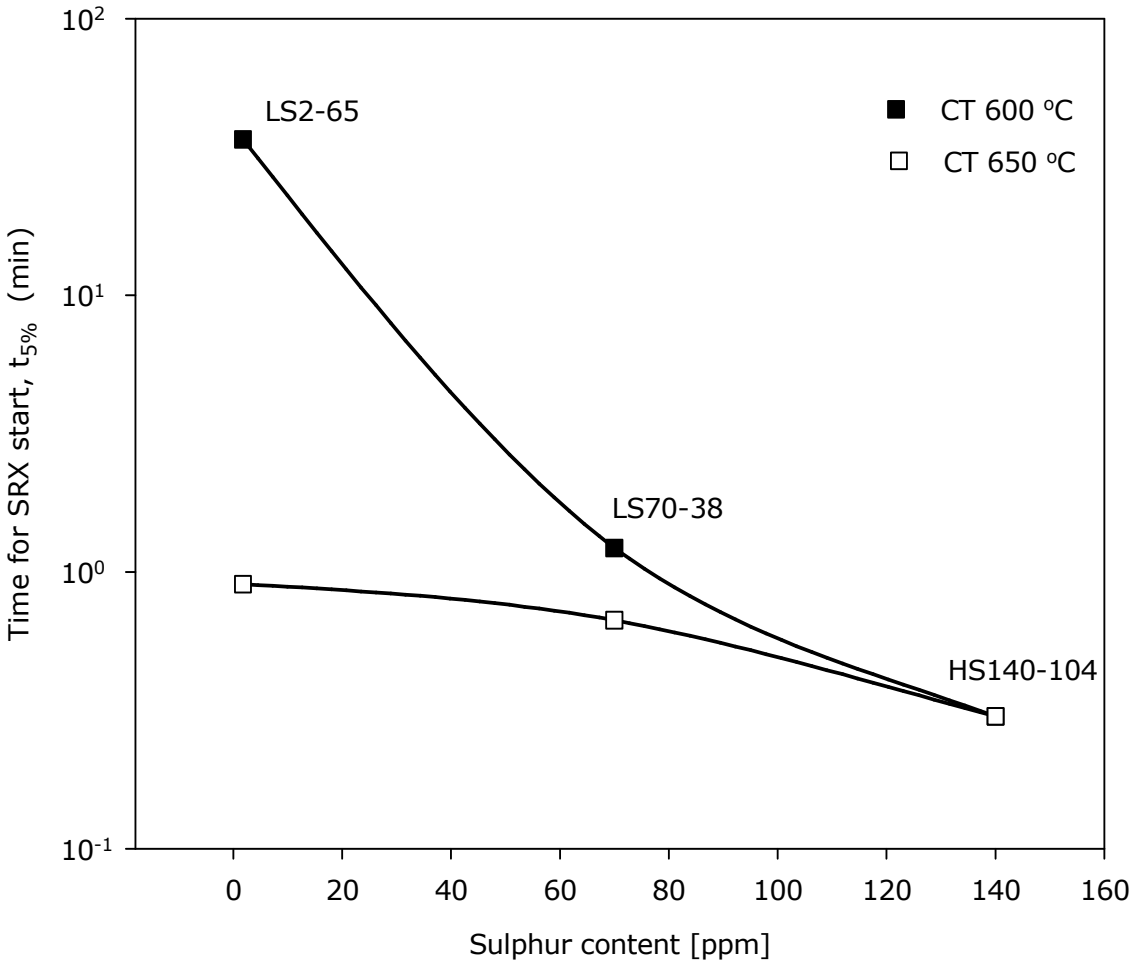

Figure 12.20: The 5 percent recrystallisation time $t_{5\%}$ in minutes, plotted as a function of the sulphur content (ppm) of the corresponding steel as labeled in the figure.

The logarithm of the recrystallisation start time $t_{5\%}$ is plotted against the sulphur content in ppm in figure 12.21. The empirical expressions for predicting the recrystallisation start time $t_{5\%}$ as a function of the sulphur content in ppm, are given in table 12.2 and these expressions have been derived from the results given in figure 12.21. It is, however, necessary to mention that these are

not universal equations; they are specific for these steels under the processing conditions specified above.

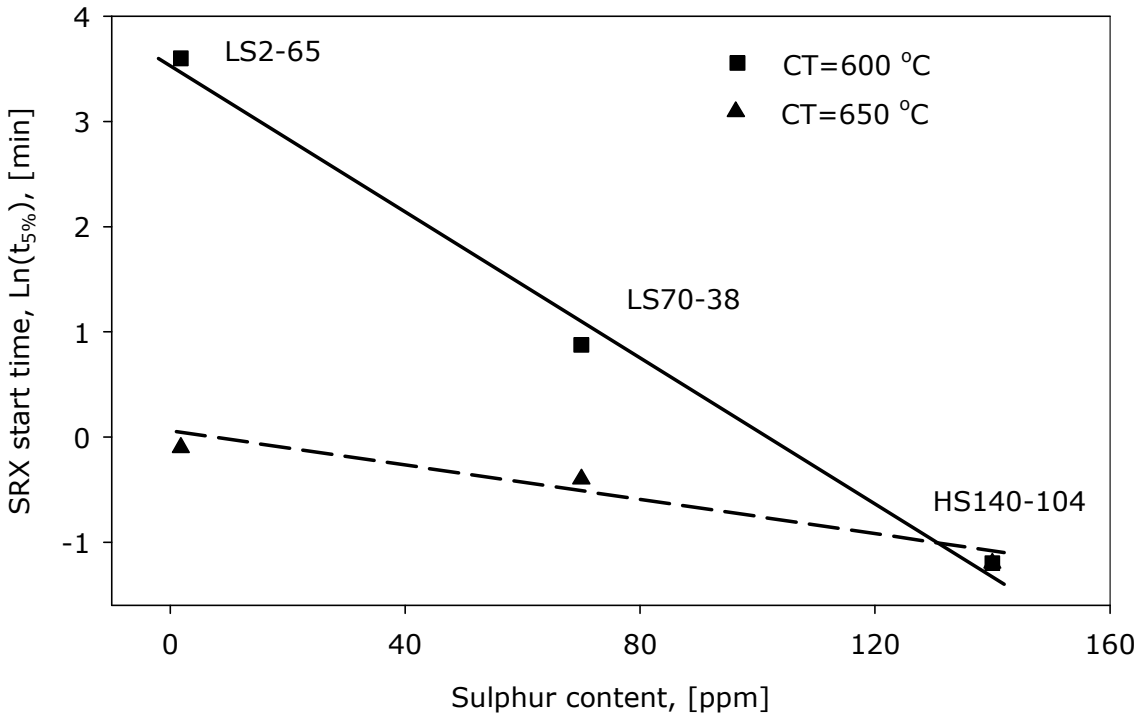

Figure 12.21: Logarithm of the static recrystallisation start time $t_{5\%}$ versus the sulphur content in ppm.

Table 12.2: Empirical expressions for predicting the recrystallisation start time $t_{5\%}$ as a function of the sulphur content in ppm derived from the results in figure 12.21 above; CT = coiling temperature.

CT (°C)	SRX $t_{5\%}$	R^2 value
600	$t_{5\%}$ = 33.78exp(-0.0345S)	0.993
650	$t_{5\%}$ = 0.99exp(-0.008S)	0.94

12.4.2 Metallographic analysis on static recrystallisation in steels HS140-104 and LS2-65

The metallographic analysis through TEM of thin foils focused on the nucleation of recrystallisation during the annealing process and the possible influence of the AlN particles on the kinetics of the recrystallisation process. Figures 12.22 to 12.24 show preferential nucleation of new recrystallised grains on subgrain boundaries and around extensively cold worked regions around Fe_3C particles in both steels HS140-104 and LS2-65. These areas provided extra driving force for the nucleation of new recrystallised grains in both low and high sulphur steels.

Figure 12.23 shows a new grain that nucleated on the deformation band in steel HS140-104, and is growing in the direction of the arrows parallel to the deformation bands while growth normal to the sides parallel to the deformation bands is probably inhibited by orientation pinning from low angle grain boundaries.

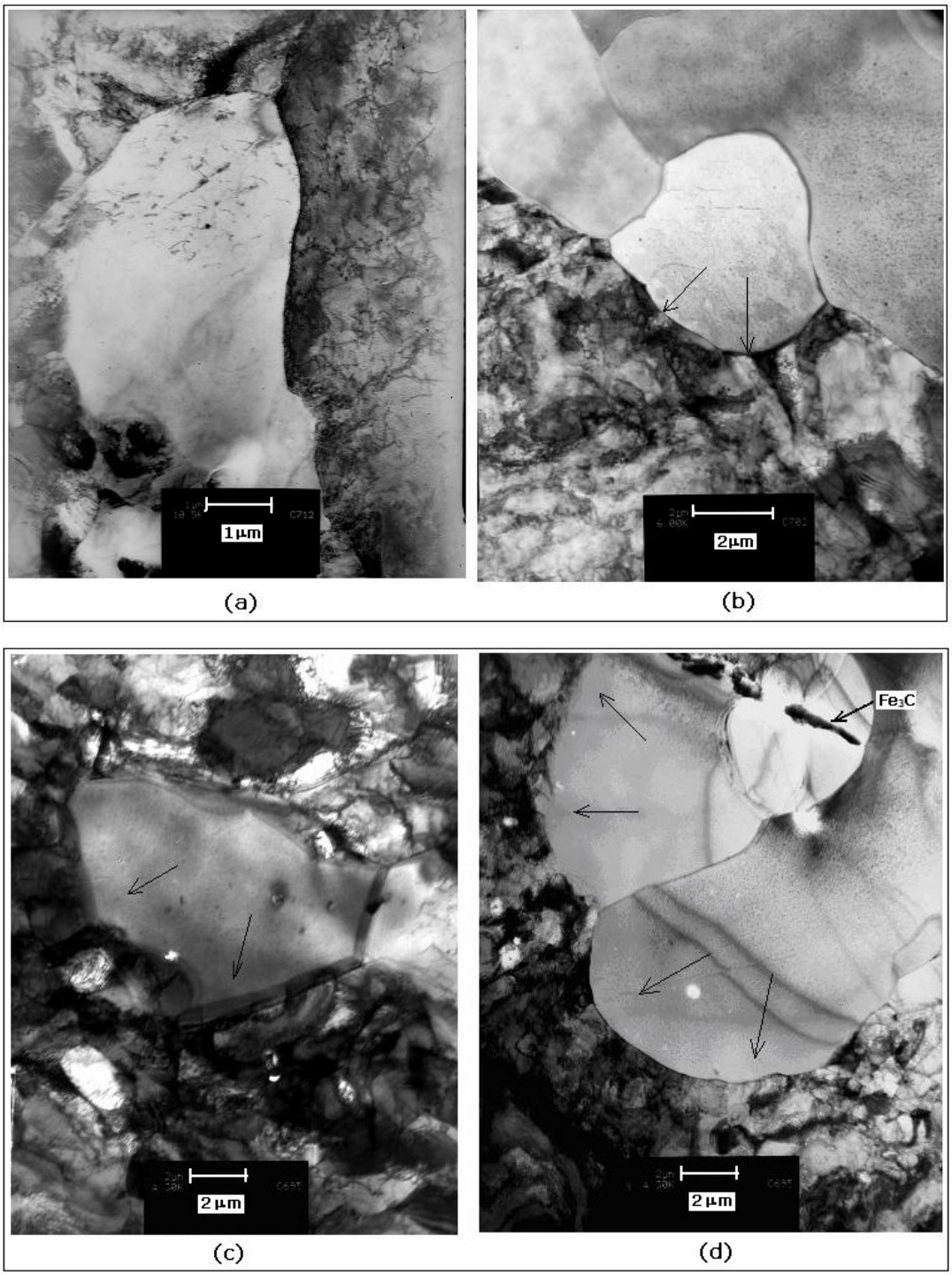

Figure 12.22: Nucleation of new recrystallised grains on subgrain boundaries growing into the deformed matrix by Strain Induced Boundary Migration (SIBM): (a) and (c) new recrystallised grains are

formed in steels LS2-65 and HS140-104 respectively while in (b) and (d) the grains are growing into the deformed matrix as indicated by the arrows in steels LS2-65 and HS140-104 respectively.

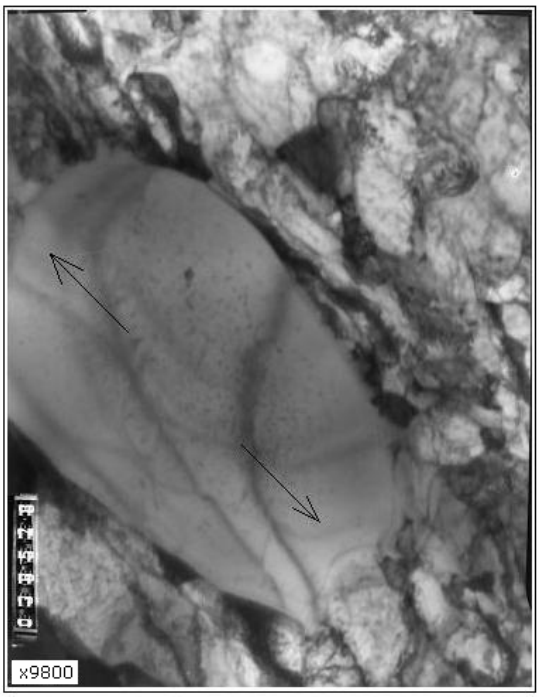

Figure 12.23: Steel HS140-104, showing a new grain that nucleated on a deformation band and is growing in the direction of the arrows parallel to the deformation bands.

Chapter 12 Results

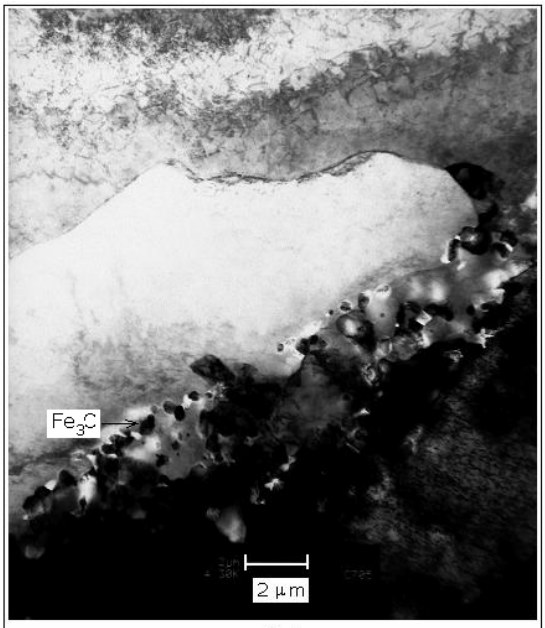

(a)

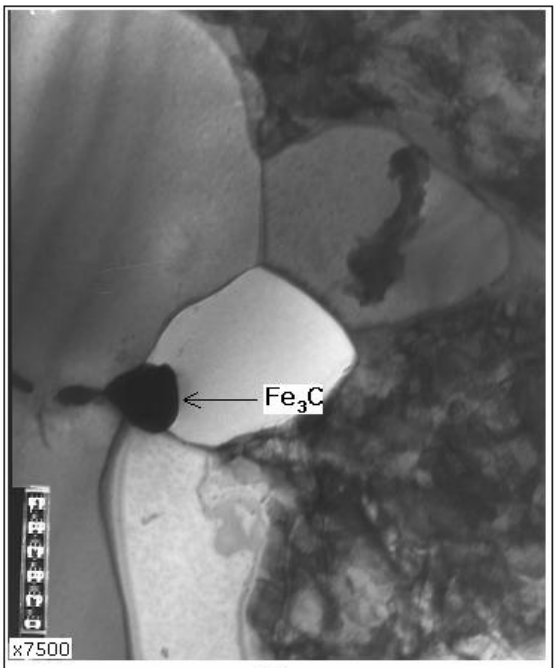

(b)

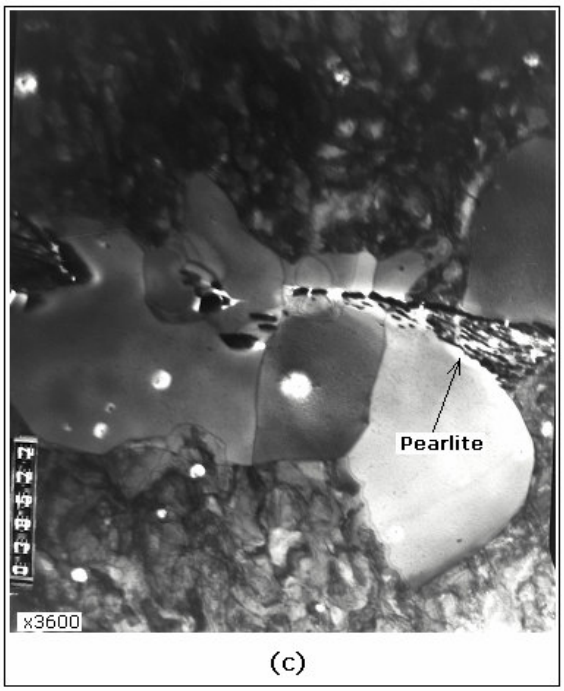

Figure 12.24: Nucleation of new recrystallised grains within extensively cold deformed regions around pearlite colonies and Fe_3C particles. (a) steel LS2-65, (b) and (c) steel HS140-104 .

Figure 12.25 shows the micrographs from TEM thin foils in which observations of the pinning interaction of AlN fine particles (< 30 nm) with the recrystallisation process in the low sulphur content steel LS2-65, were made. The wavy recrystallisation front observed in figure 12.25 (a) shows the pinning effect of the fine AlN precipitates in the low sulphur steel LS2-65 which, consequently, retards the recrystallisation process in this steel. More evidence of the pinning of the recrystallisation front by the Zener drag effect is seen in the micrographs in figures 12.25 (b) and (c) which were taken at higher magnification. The same investigation was done on the higher sulphur content steel HS140-

Chapter 12 Results

104 and no particle pinning of the recrystallisation front was observed, see figure 12.26 below.

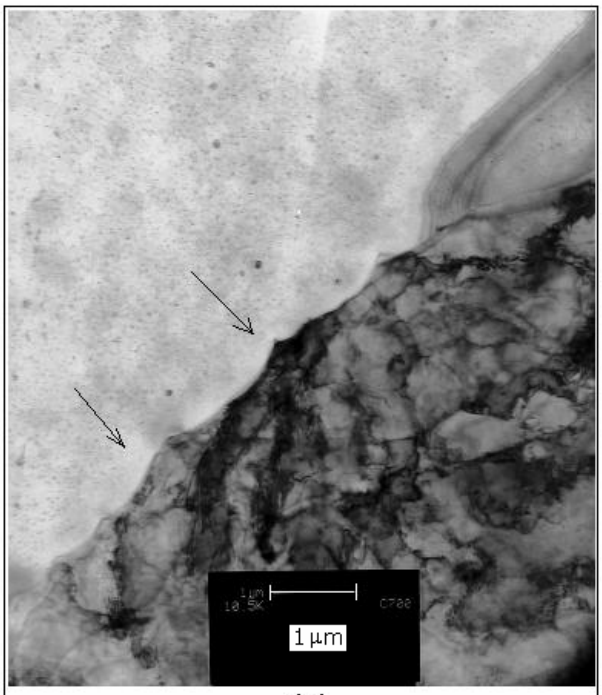

(a)

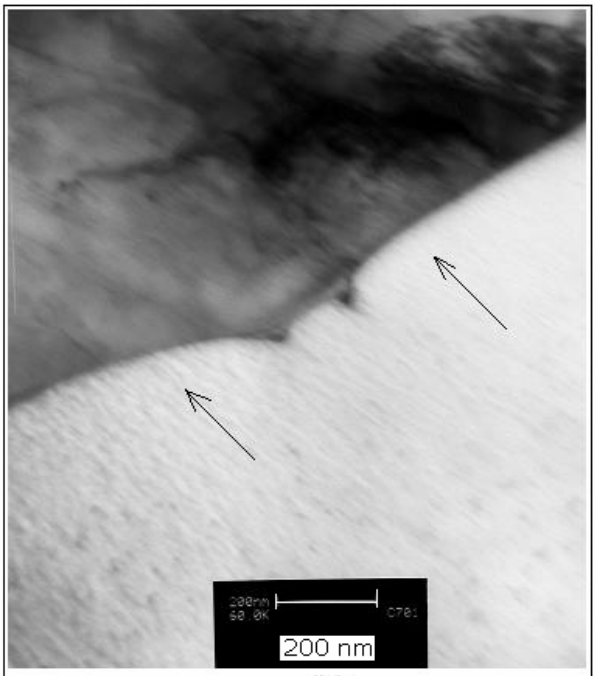

(b)

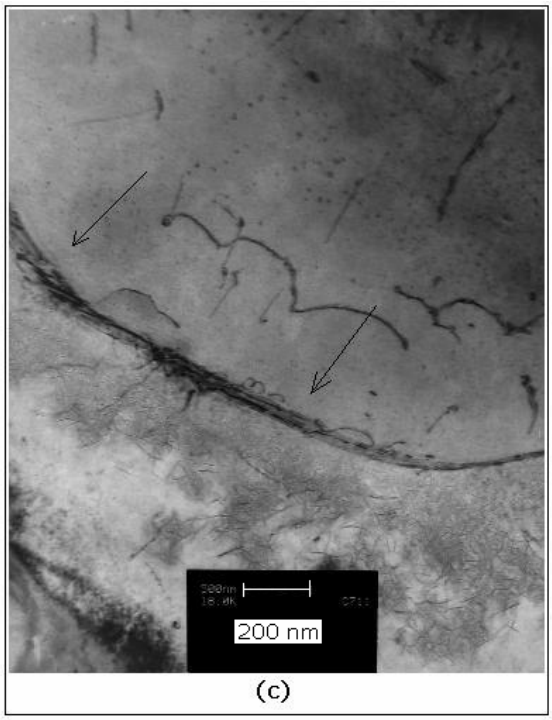

(c)

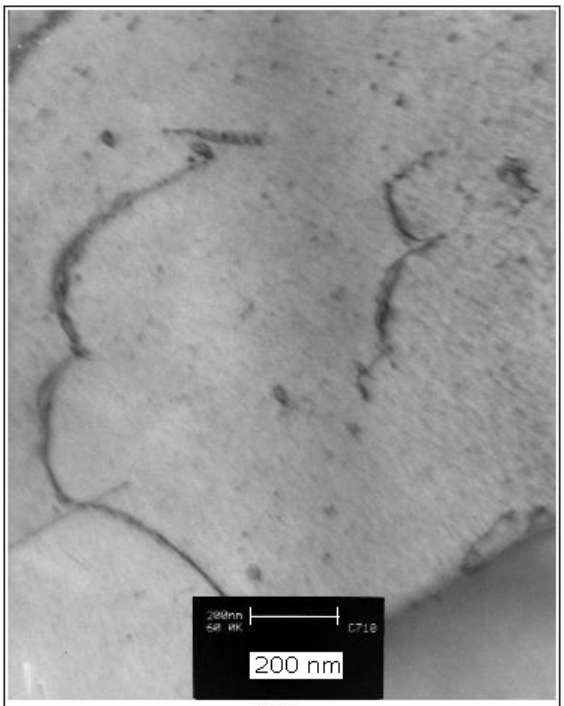

(d)

Figure 12.25: Particle pinning of recrystallisation (SRX) in steel LS2-65: (a) a wavy recrystallisation front, (b) particle pinning of the SRX front by two AlN particles which were about 100 nm apart, (c) dislocation

pinning in and around the SRX front and (d) dislocations pinned by AlN particles just behind the SRX front.

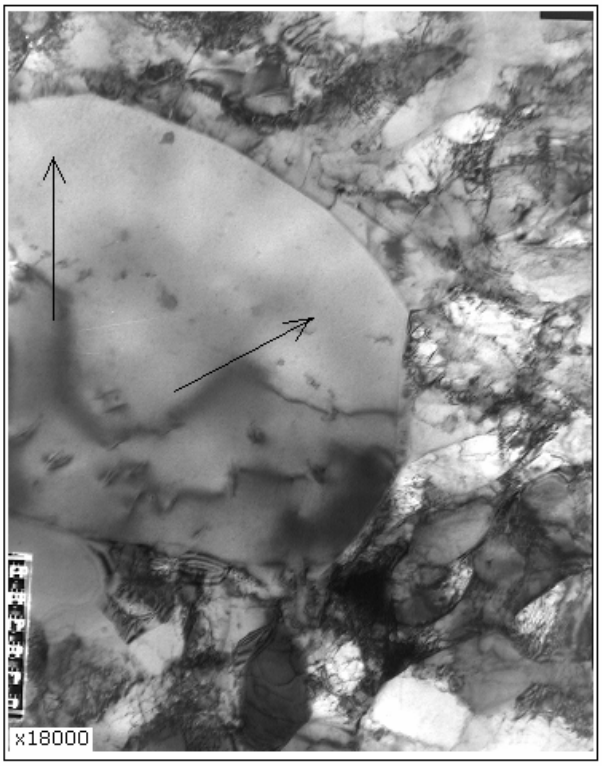

Figure 12.26: Recrystallisation front that is growing into the deformed matrix without encountering particle pinning in higher sulphur steels HS140-104.

12.5 Precipitation of AlN on MnS and the resulting mean particle size of the former

Steels HS140-104 and LS2-65, one with high and the other with low sulphur contents respectively were hot rolled and coiled in the Gleeble 1500^{TM} according to the schedule and heat treatment cycle specified in table 11.1 and figure 11.1 respectively. The TEP measurements were carried out according to the procedure given in section 10.5.

12.5.1 TEP measurements in an as-coiled condition

The absolute TEP measurements were taken from eight specimens which were obtained from each of the steels and the results are given in table 12.3 below. As may be seen in table 12.3 and figure 12.27, there was no significant change in the absolute TEP values immediately after coiling and after isothermal annealing at 800 for 2 hours. This was evidence that there was no further significant precipitation of AlN, in both steels, after hot rolling and coiling for 1 hour at 600 °C in a Gleeble 1500^{TM} simulator.

Chapter 12 Results

Table 12.3: Absolute TEP values for the steels LS2-65 and HS140-104 which were solution treated at 1150 °C for 10 minutes, hot rolled in 4 passes and then coiled at 600 °C for 1 hour; TEP1 = absolute TEP value immediately after coiling while TEP2 = absolute TEP value after annealing at 800 °C for 2 hours cooled to 600 °C and annealed for 10 minutes and quenched in water. Error = 0.033 μV K^{-1}.

Specimen	Steel LS2-65		Steel HS140-104	
	TEP1 μV/K	TEP2 μV/K	TEP1 μV/K	TEP2 μV/K
1	9.21	9.10	9.40	9.40
2	9.20	9.14	9.26	9.14
3	9.14	9.00	9.31	9.32
4	9.28	9.06	9.28	9.38
5	9.10	9.12	9.10	9.23
6	9.06	9.00	9.16	9.17
7	9.21	9.20	9.10	9.21
8	9.10	9.10	9.07	9.00
Mean	9.16	9.09	9.21	9.23
Std. dev.	0.07	0.07	0.12	0.13

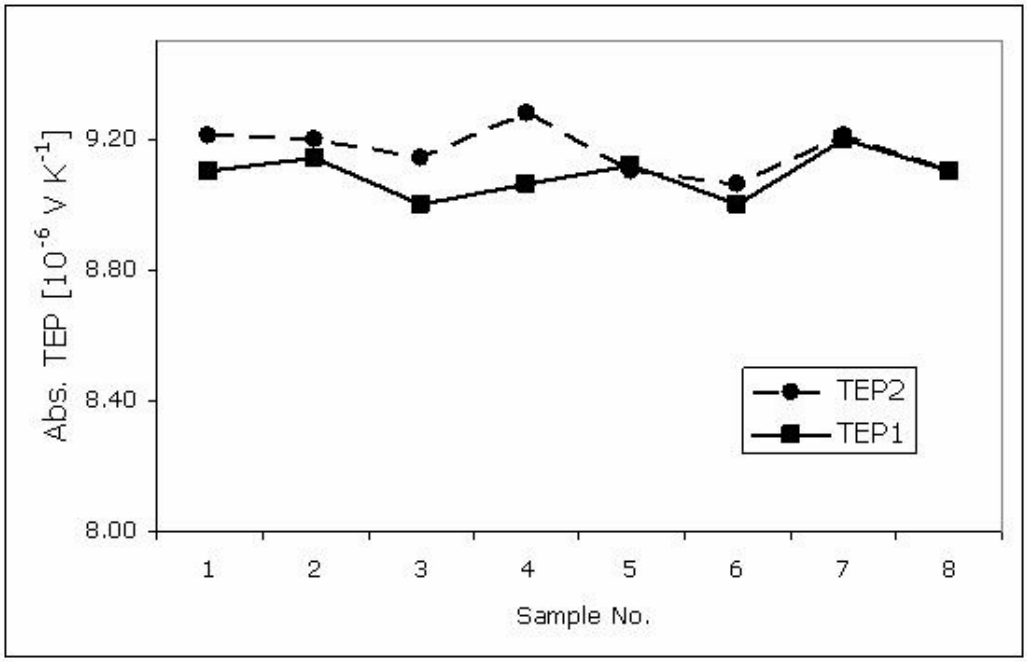

(a)

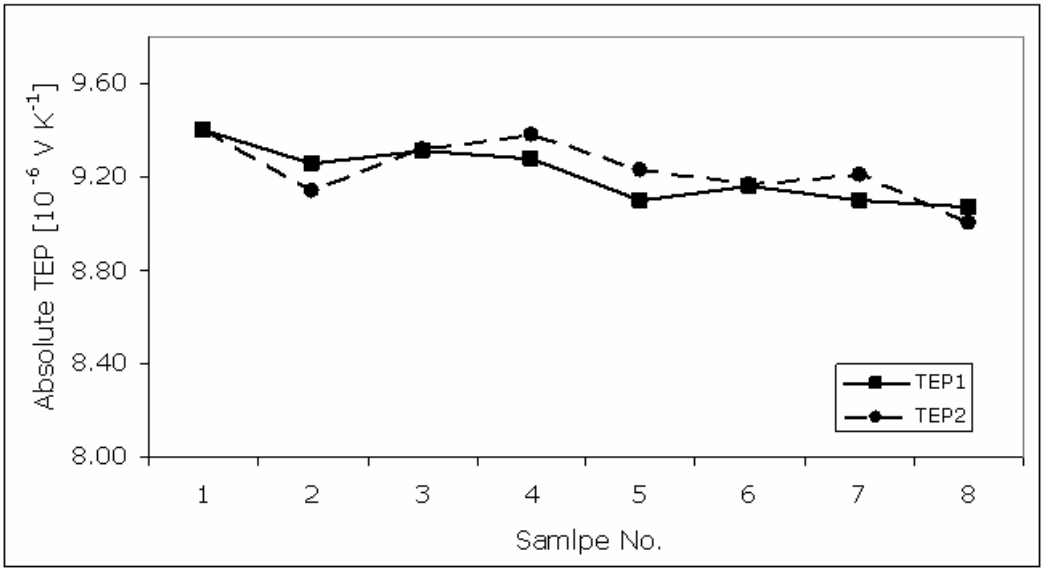

(b)

Figure 12.27: Absolute TEP measurements for the as-coiled condition of steels (a) LS2-65 and (b) HS140-104 where TEP1 and TEP2 are as defined in table 12.2 above.

12.5.2 Precipitation of AlN during hot rolling and coiling simulations

Metallographic analysis was carried out on steels HS140-104, LS70-38 and LS2-65 in the hot deformed and as-coiled condition in the Gleeble 1500^{TM} in order to investigate the possible influence of the sulphur content on the precipitation of AlN during coiling at 600 and 650 °C. The hot rolling and coiling schedules were given in table 11.1 and figure 11.1. The results from the metallographic analysis are given in figures 12.28 to 12.31.

It was observed that in the higher sulphur content steel HS140-104, the AlN was associated with MnS and [Mn,Cu]S, see figures 12.28 (b) and (c) below, and the particles were generally coarse between 50 and 300 nm in size. In the medium sulphur content steel LS70-38, the AlN was also associated with [Mn,Ti,V]S complex sulphides but the particles were relatively finer compared with steel HS140-104, between 50 and 100 nm, see figure 12.29. In the lowest sulphur content steel LS2-65; no AlN could be observed on extraction carbon replicas as this technique is not sensitive enough to reveal the very fine particles and, therefore TEM thin foils were used. Through this technique fine AlN particles (< 30 nm) were observed and these were not associated with the MnS as there was none due to the very low sulphur content of only 2 ppm in this steel, see figure 12.30 below.

Chapter 12 Results

The main observation here was that the heterogeneous association of AlN with the MnS in medium to high sulphur content steels, modified the effective particle size of the former if compared with the low sulphur content steels in which the AlN nucleated homogeneously in the matrix or heterogeneously on grain boundries as shown in figures 12.30 and 12.31 respectively. This difference in effective particle size of the AlN between the higher and the lower sulphur content steels contributed later to the difference in the recrystallisation behaviour of these two groups of steels i.e. it is generally "sluggish" in the lower sulphur content steels due to presence of much finer AlN particles which may pin the dislocation sub-boundaries and the static recrystallisation fronts through Zener drag.

The mean particle size for steels HS140-104, LS70-38 and LS2-65 was measured from approximately one hundred particles and their mean is plotted against the sulphur content of their respective steels in figure 12.32. The error bars represent the standard deviation from the diameter measurements. The main observation in figure 12.32 was that the 5 percent recrystallisation time $t_{5\%}$ increased as the mean particle size decreased with the decrease in sulphur content of the steel.

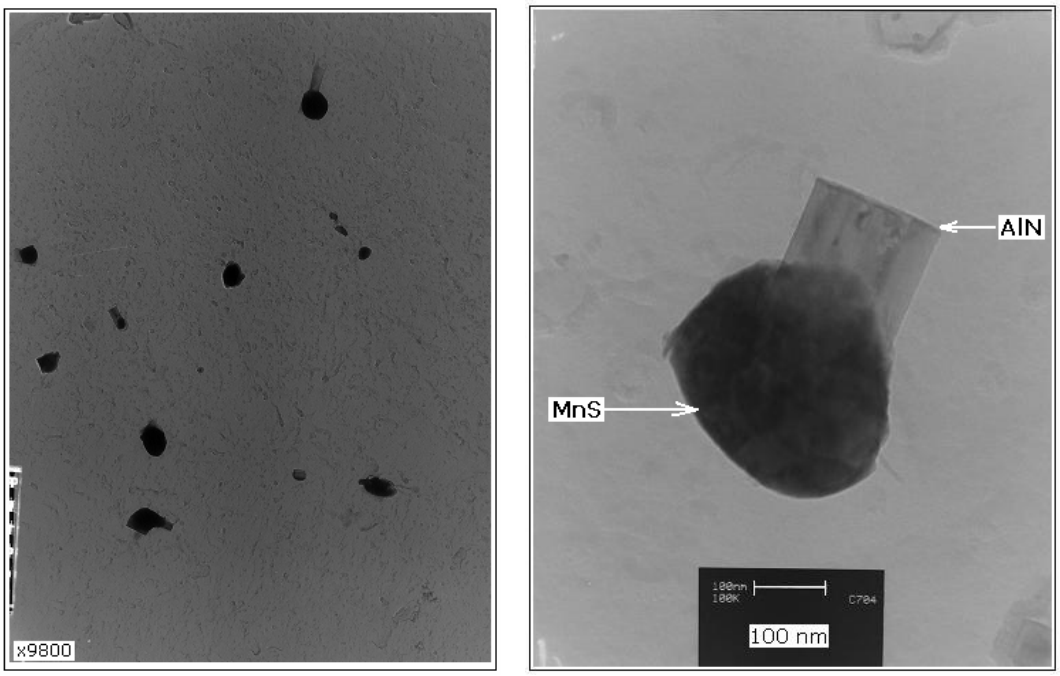

(a) (b)

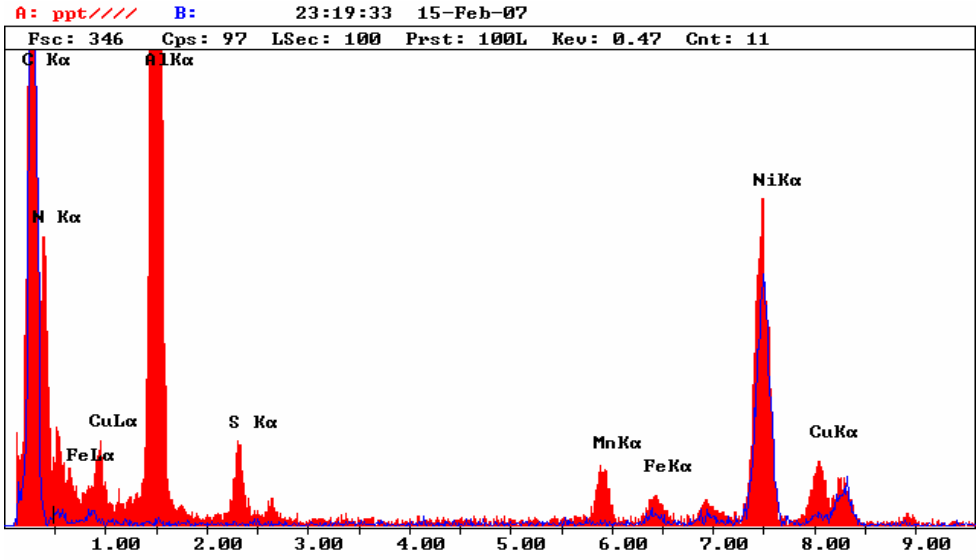

(c)

Figure 12.28: TEM replica micrographs and EDS spectrum for the higher sulphur content (140 ppm) steel HS140-104 in the as-coiled condition, hot rolled and coiled at 600 °C. (a) AlN particles observed at low magnification, (b) about 150 nm particle in micrograph (a) now

observed at higher magnification, (c) EDS spectrum of the particle in micrograph (b).

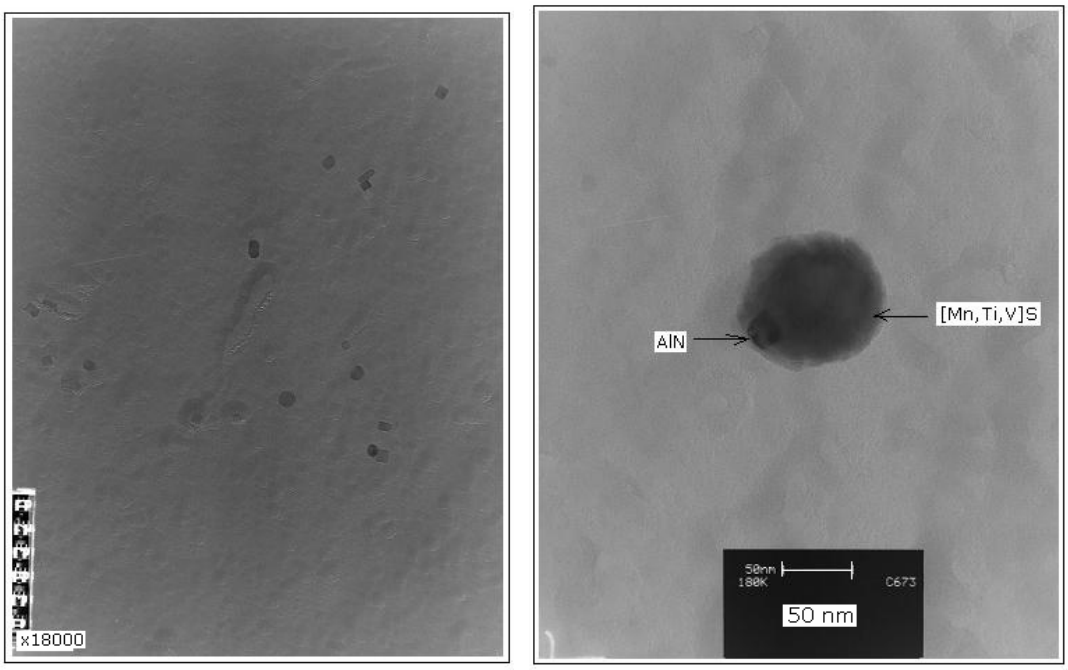

(a) (b)

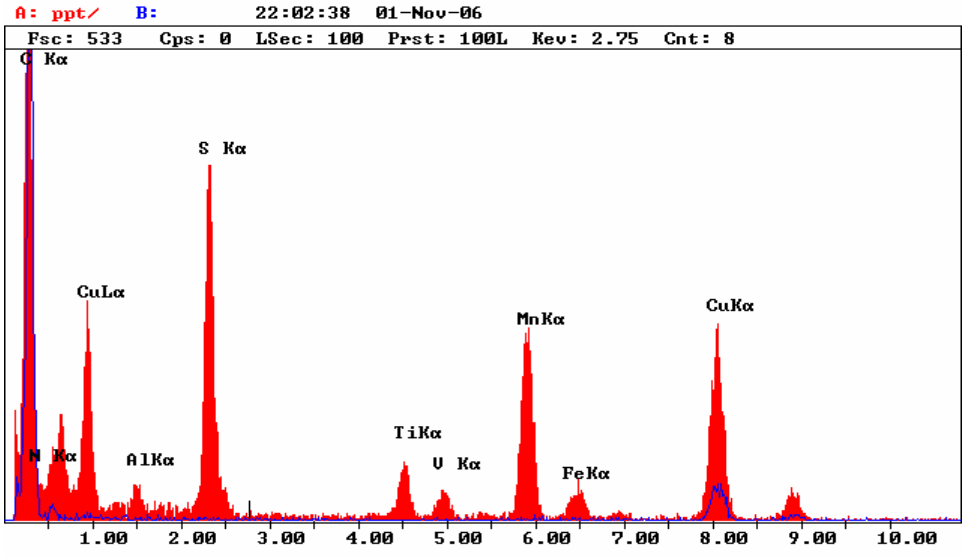

(c)

Figure 12.29: TEM replica micrographs and EDS spectrum for the medium sulphur content (70 ppm) steel LS70-38 in the as-coiled condition, hot rolled and coiled at 600 °C. (a) AlN particles observed at low magnification, (b) about 80 nm particle in micrograph (a) now

observed at higher magnification, (c) EDS spectrum of the particle in micrograph (b).

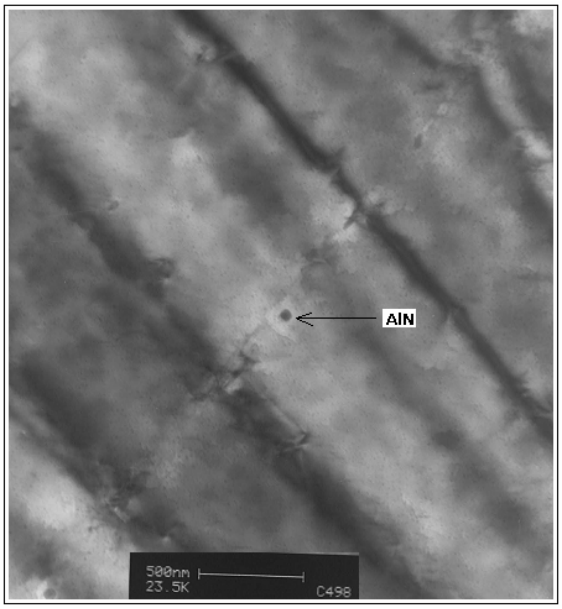

(a)

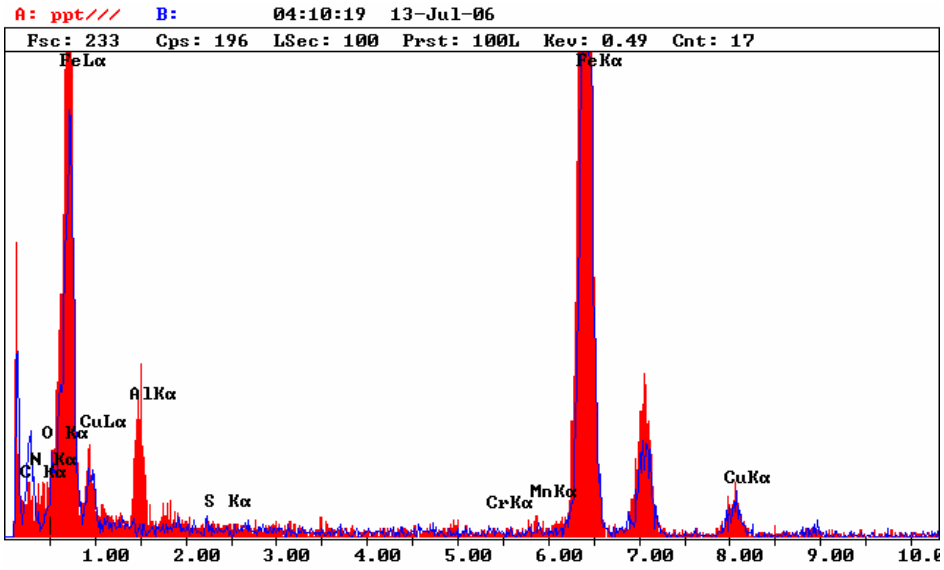

(b)

Figure 12.30: TEM thin foil micrograph and EDS spectrum for the low sulphur content steel LS2-65 in the as-coiled condition, hot rolled and

coiled at 600 °C. (a) micrograph showing a typical AlN particle, (b) the EDS spectrum for the particle in (a).

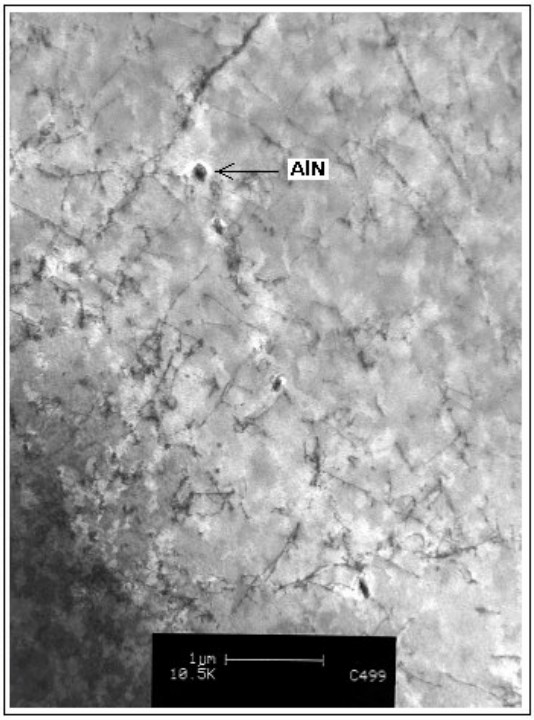

(a)

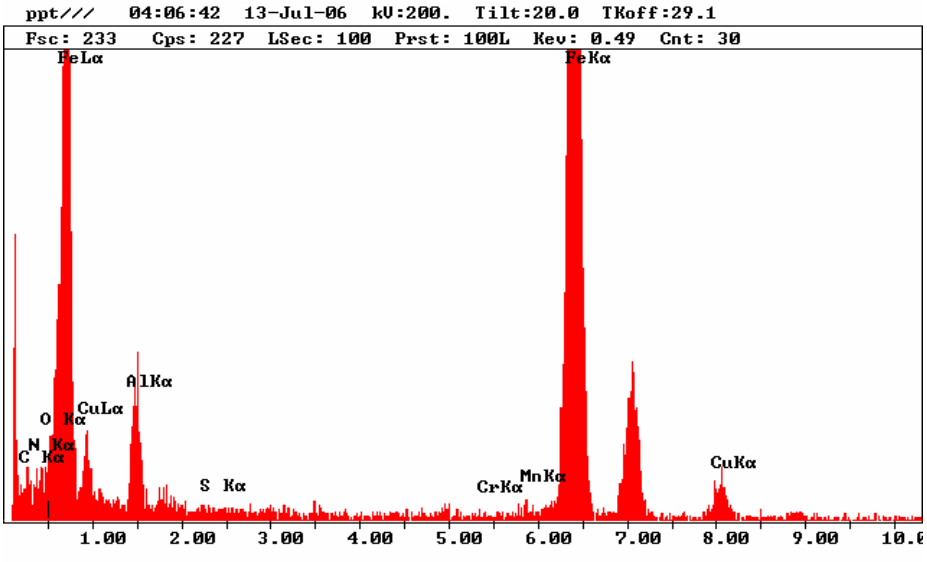

(b)

Figure 12.31: (a) TEM thin foil micrograph showing precipitation of AlN on prior grain boundary and on dislocations and (b) EDS spectrum of the AlN particles that were observed in (a) for the low sulphur content

steel LS2-65 in the as-coiled condition, hot rolled and coiled at 650 °C for 1 hour.

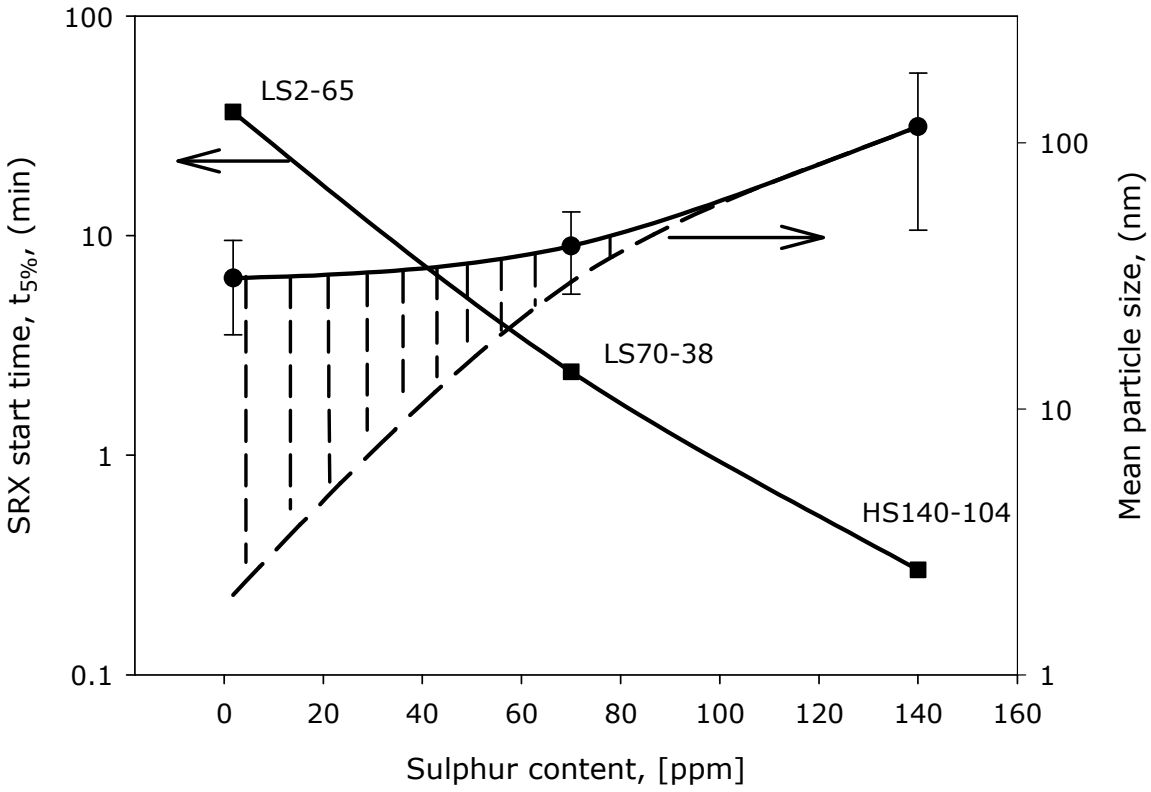

Figure 12.32: The recrystallisation start time $t_{5\%}$ and the AlN mean particle size as measured from thin foils, are plotted as a function of the sulphur content in steels HS140-104, LS70-38 and LS2-65. The cross hatched area represents possible particles that were "missed" due to a lower limit of detection of about 20 nm by thin foil TEM.

12.5.3 Crystallographic orientation relationship between AlN and MnS

As mention earlier in section 11.3.1, the TEM camera constant was calibrated using a gold film and from which the lattice parameter for the AlN and the MnS were found to be 0.318 and

0.529 nm respectively. This was in reasonable agreement with literature values where the lattice parameters for AlN and MnS were found to be 0.311 and 0.522 nm respectively[36,48].

The compound MnS/AlN particle and the electron diffraction patterns for the AlN, MnS and the compound particle are given in figure 12.33. The zone axis for the AlN was $[2\bar{1}\bar{1}0]$ while that for the MnS was [110]. The orientation relationship between the AlN and the MnS was found to be $(1\bar{1}1)_{MnS}//(0001)_{AlN}$ and $[110]_{MnS}//[2\bar{1}\bar{1}0]_{AlN}$ which agrees with the observation of Ushioda et al[52] in a 0.036%C steel with 150 ppm sulphur and 41 ppm nitrogen. The schematic diagram of the electron diffraction pattern for the compound particle is given in figure 12.33 (e) below.

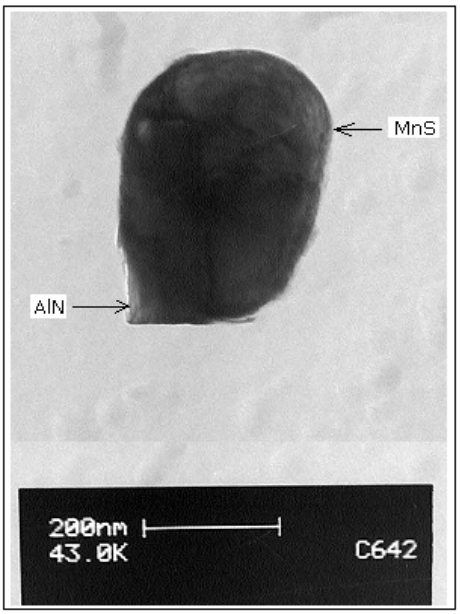

(a)

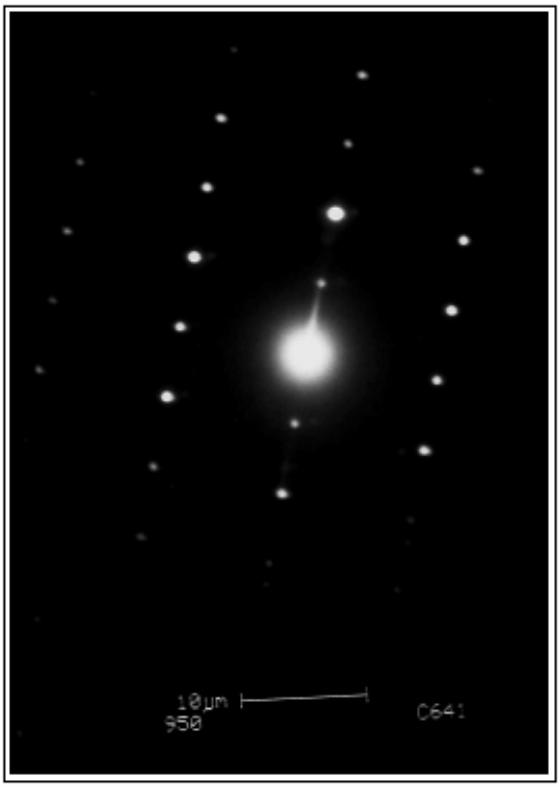

(b)

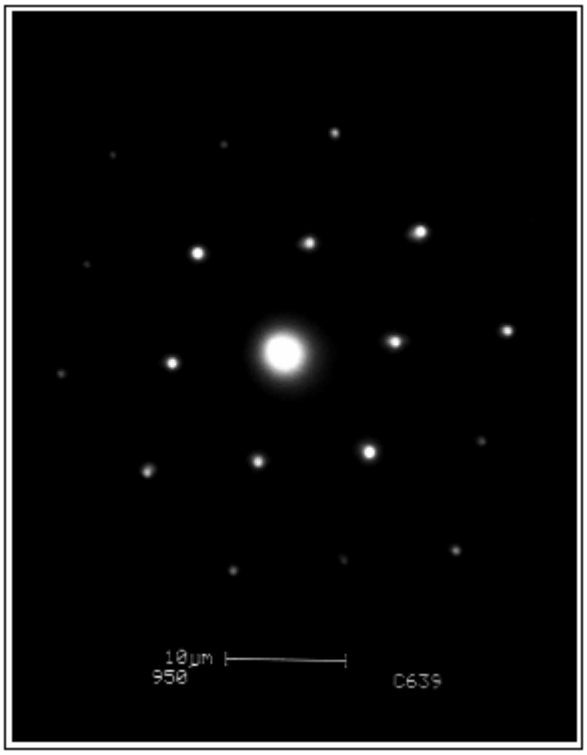

(c)

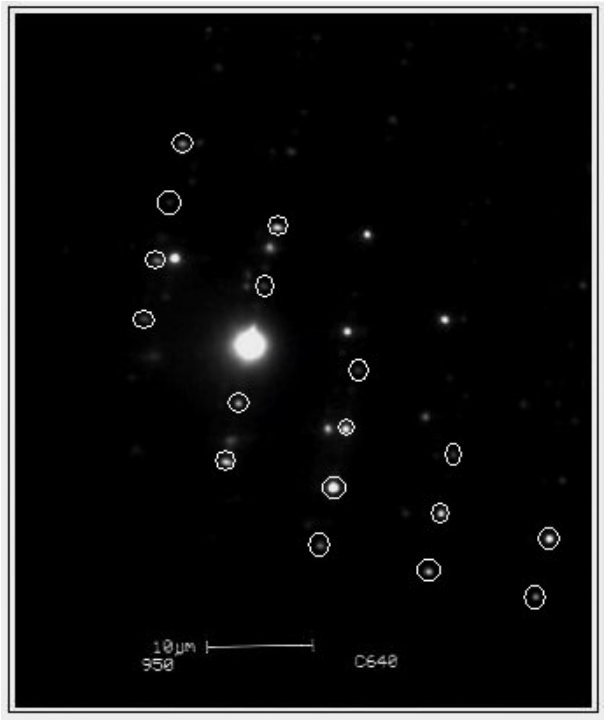

(d)

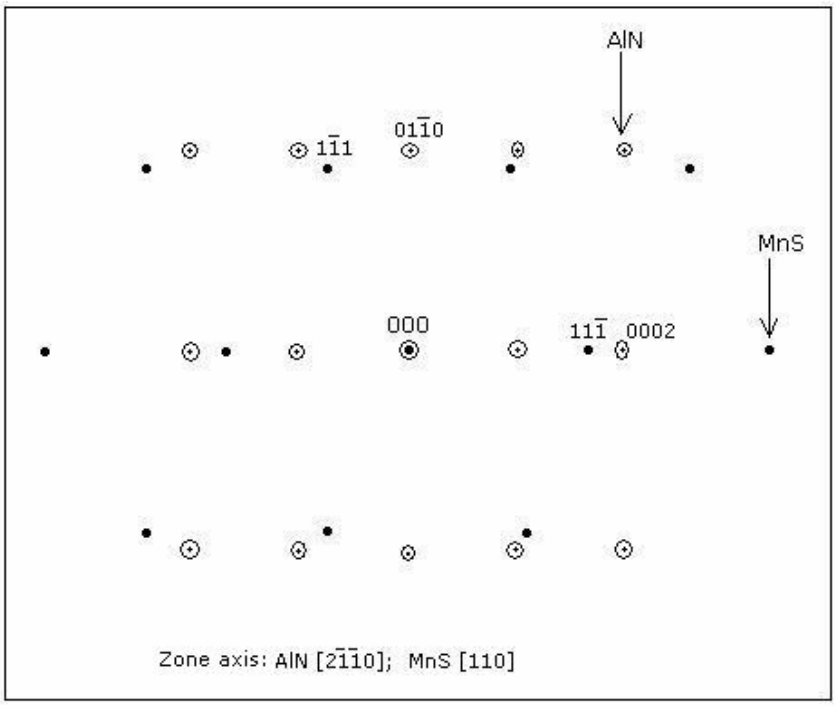

(e)

Figure 12.33: Crystallographic orientation relationship between AlN and MnS: (a) an AlN particle that nucleated on MnS (b) diffraction pattern

of AlN on $[2\bar{1}\bar{1}0]$ zone axis, (c) diffraction pattern of MnS on $[110]$ zone axis, (d) diffraction patterns of both AlN (in open symbols) and MnS (in solid symbols) (e) schematic diagram of the diffraction pattern in (d) with $(1\bar{1}1)_{MnS}//(0001)_{AlN}$, $[110]_{MnS}//[2\bar{1}\bar{1}0]_{AlN}$.